

Manuscript Number: HE-D-18-02260R1

Title: Pt nanowire growth induced by Pt nanoparticles in application of the cathodes for Polymer Electrolyte Membrane Fuel Cells (PEMFCs)

Article Type: Full Length Article

Section/Category: Fuel Cells & Applications

Keywords: Pt nanowire; cathode; PEMFC; growth; tailoring; architecture.

Corresponding Author: Professor Sheng Sui, Ph. D

Corresponding Author's Institution: Shanghai Jiao Tong University

First Author: Sheng Sui, Ph. D

Order of Authors: Sheng Sui, Ph. D; Zhaoxu Wei; An He; Kaihua Su; Xiaoying Wang; Yuehong Su, Ph. D; Xianghui Hou, Ph. D; Saffa Riffat, Ph. D; Shangfeng Du, Ph. D

Abstract: Improving cathode performance at a lower Pt loading is critical in commercial PEMFC applications. A novel Pt nanowire (Pt-NW) cathode was developed by in-situ growth of Pt nanowires in carbon matrix consisting Pt nanoparticles (Pt-NPs). Characterization of TEM and XRD shows that the pre-existing Pt-NPs from Pt/C affect Pt-NW morphology and crystallinity and Pt profile crossing the matrix thickness. The cathode with Pt-NP loading of 0.005 mgPt-NP cm<sup>-2</sup> and total cathode Pt loading of 0.205 mgPt cm<sup>-2</sup> has the specific current density of 89.56 A gPt<sup>-1</sup> at 0.9V, which is about 110 % higher than that of 42.58 A gPt<sup>-1</sup> of the commercial gas diffusion layer (GDE) with Pt loading of 0.40 mg cm<sup>-2</sup>. When cell voltage is below 0.48V, the Pt-NW cathode has better performance than the commercial GDE. It is believed that the excellent performance of the Pt-NW cathode is attributed to Pt-NP induction, therefore producing unique Pt-NW structure and efficient Pt utilization. A Pt-NW growth mechanism was proposed that Pt precursor diffuses into the matrix consisting of pre-existent Pt-NPs by concentration driving, and Pt-NPs provide priority sites for platinum depositing at early stage and facilitate Pt-NW growth.

Dear Editor Dr. Shohji Tsushima,

Many thanks for your and reviewers' very helpful comments. We have made revisions and corrections according to their comments and suggestions. We have marked all the changes in revised mode in the revised manuscript, and made the following responses(Green) to the comments(Black).

Two references from *Int. J. Hydrogen Energy* was added as the literature survey updating.

We also added an acknowledgement on the International Science & Technology Cooperation Program of the Ministry of Science & Technology (grant No. 2015DFG62250) .

We believe the revised manuscript meets the journal quantity and will have good response.

Thank you very much again!

Sincerely yours,

Sheng SUI

Suggested reviewers

1. Shaojun GUO, Peking University, [guosj@pku.edu.cn](mailto:guosj@pku.edu.cn)
2. Ramaraja P. Ramasamy, University of Georgia, [rama@uga.edu](mailto:rama@uga.edu)
3. Sara Cavaliere, Institut Charles Gerhardt, [sara.cavaliere@umontpellier.fr](mailto:sara.cavaliere@umontpellier.fr)

## Response to reviewers

We thank the Referees for their very helpful comments. We have made revisions and corrections according to their comments and suggestions. We have marked all the changes **in revised mode** in the revised manuscript, and made the following responses(**Green**) to the comments(**Black**).

Reviewers' comments:

**Reviewer #1:** The authors have reported very good work in this manuscript. This manuscript may be accepted in the IJHE. More ever, the reviewer observation is given here below.

1)The introduction section is too long, it should be precise and short .

[Following Reviewer #1's suggestion, the introduction section is refined.]

2)"Pt nanoparticles pre-existing in the carbon matrix improve growth"... ..Authors should justify the reason behind this improvement in terms of reaction kinetics if any.

[In the section 3, the mechanism of Pt nanowires growing on Pt nanoparticle seeds is proposed and discussed in the details. Polarization and EIS experiments were carried out to further evaluate the cathodes performances(oxygen reduction reaction kinetics).]

3)"The cathode with Pt-NP loading of 0.005 mgPt-NP cm<sup>-2</sup> and total cathode Pt loading of 0.205 mgPt cm<sup>-2</sup> has the specific current density of 89.56 A gPt<sup>-1</sup> at 0.9V, which is about 110 % higher than that of 42.58 A gPt<sup>-1</sup>"..... Authors are requested to represent the current density with respect to area.

[Data of the specific current density with respect to area were added in Table 1 in the revised manuscript. ]

4)"our further studies on the matrix materials shows that, comparing with the 4 carbon matrix, the Pt-NWs growing in a Pt/C matrix displayed shorter length and "fluff" on the carbon support".....this sentence should be rewrite.

[The above sentence was rewritten as " Our further studies on effects of the matrix materials shows that, comparing with the carbon matrix, the Pt-NWs growing in a Pt/C matrix display shorter and denser fluff on the carbon support." in the revised manuscript]

5) Instead of adding Pt/C , if you add directly only Pt nanoparticles what would happen in the growth of Pt NW? Moreover, describe the role of carbon support in the Pt-NW growing mechanism.

[Only Pt nanoparticles cannot achieve on the similar result as the ones supported on carbon. The carbon support provides surface to disperses the Pt nanoparticles. Reported from our previous work (K Su, *Fuel Cells*, 2015, 15(3), 449), the Pt-NWs growing in a pure Pt/C matrix are shorter and denser fluff than that in a carbon matrix. Therefore, in this paper a mixture of Pt/C and carbon was used to alleviate dense Pt-NWs fluff.]

6) "Nafion® perfluorinated resin solution (ionomer) (DE1020, 10% by wt.)" .....

Author are requested to write 10 wt.% instead of 10% by wt. to maintained uniform style throughout the manuscript.

[It was corrected in the revised manuscript.]

7) Authors are requested to check the fuel cell performance using developed catalyst at the cathode as well as at the anode.

[The home-made cathode and the anode were prepared by decal transfer process while all anodes are the same made of commercial Pt/C catalyst, which is clearly described in the manuscript. We could not understand the reviewer's requirement on checking the fuel cell performance.]

8) What about the stability for the developed catalyst?

[As introduced in literature reviewing part, Pt-NWs supported on carbon black are characterized for enhanced stability due to their "lower vulnerability to dissolution, Ostwald ripening, and aggregation than those of Pt nano particles (NPs).<sup>1,12,14</sup>" in electrochemical cells. We will investigate the stability and durability for the developed catalysts in the matrix in fuel cell configuration later.]

9) The comparison of current density of the developed catalyst should be reported at the potential range of 0.4-0.6 V, which is fuel cell operating range under the applied load, instead of at 0.9 V.

[In order to minimize mass transport resistances, the comparison of current density, or activity, of the developed catalyst is carried out under high potential range, usual at 0.9V.]

10) From the fig. 5(a) it can be clearly seen that the area under the curve for the H adsorption for Pt-NP 0 and Pt-NP 0.005 is almost same. However, the ECSA is reported significantly higher for Pt-NP 0.005 as compared to Pt-NP 0, what is reason?

[The electrochemical active surface areas (ECSAs) of Pt nanowires electrodes were calculated on the hydrogen adsorption area from 0.1 to 0.4 V of the CV data. The three peaks for Pt-NP 0, Pt-NP 0.005 and Pt-NP 0.010 are partly overlapping. The areas under the curve for the H adsorption for Pt-NP 0 and Pt-NP 0.005 are 0.3905 and 0.4337, although they seem almost same. So the calculation results are correct]

**Reviewer #2:** The introduction is well done and complete, the proposed Pt growth mechanism is well justified. The applicative results with the synthesized catalyst are not so satisfying when compared to standard commercial material.

[The polarization curves of various single cells with the commercial GDE and home-made Pt-NW cathodes are shown in Fig. 3. The Pt loading ratio of the optimal Pt-NW cathode and the commercial cathode is  $0.205 \text{ mg}_{\text{Pt}} \text{ cm}^{-2}$  vs  $0.40 \text{ mg}_{\text{Pt}} \text{ cm}^{-2}$ . The home-made electrode is with about half loading of the commercial while their cell performance is similar. It is obvious that the former is better than the latter]

More effort needs to be put in looking for distinguishing features of this approach (durability? chemical degradation? Pt agglomeration reduction?).

[We will investigate the stability and durability for the developed catalysts in the matrix in fuel cell configuration later.]

The advantage described at low voltage is not representing a real advantage since the operating conditions are far from what automotive or stationary fuel cell application is looking for (0.6 V minimum).

[We acknowledge that the present work does not get to its best performance and more space in performance improvement can be expected. Due to unusual microstructure of the Pt-NW electrode and better performance under high over potential, this can contribute to the electrode design and optimization. ]

Few typos on page 3 (check pt instead of Pt repeated several times).

[The typos on page 3 as well as the others in the manuscript were corrected.]

**Reviewer #3:** The synthesis of Pt NW induced by Pt nanoparticles in Pt/C as catalysts for PEM fuel cells is an interesting method to increase the Pt utilization. The TEM analysis indicates the uniform growth and distribution of Pt NWs and the cell performance also indicates the increased utilization efficiency of synthesized Pt NW on Pt NP electrodes. However, for fuel cell application, stability of the Pt based catalysts is most important, which is not addressed in the paper.

[Pt-NWs are more stable than Pt nanoparticles both in characteristic structure and experimental results reported elsewhere. In present paper, we focus on effects of Pt nanoparticles and the Pt-NW growth mechanism related, and will investigate the stability and durability for the developed catalysts in the matrix in fuel cell configuration later.]

The paper is of interesting and important for the development of efficient Pt based catalysts for PEMFCs but additional data on Pt NW induced by Pt NPs needs to be provided.

[We investigated the effects of Pt nanoparticles and the matrix thickness on crystal structure, size and morphology of Pt-NWs, and compared the Pt-NWs performances with a commercial electrode one. This result is sufficient to support our conclusion.]

**Reviewer #4:** In this paper, the authors present the results of their research dealing with Pt nanowire (Pt-NW) cathodes developed by in-situ growth of Pt nanowires in carbon matrix containing Pt nanoparticles (Pt-NPs). Physical and analytical characterizations were carried out, as well as, the electrochemical characterization in single fuel cell. The polarization curves indicate that when cell voltage is below 0.48V, the Pt-NW cathode has better performance than commercial gas diffusion electrode, due to the induction of Pt-NP. Finally, a Pt-NW growth mechanism was proposed.

First of all, it is worth to mention that the concept of this paper was already presented by the authors in previous studies. From this point of view, this job lacks of novelty.

[In the introduction section, we describe how present topic is developed. Inspired by our previous work (K Su, *Fuel Cells*, 2015, 15(3), 449) that Pt-NWs growing in a pure Pt/C matrix are shorter and denser fluff than that in a carbon matrix, here a mixture of Pt/C and carbon was used to alleviate dense Pt-NWs fluff and the expected results were achieved. Similar investigation was not found yet.]

I guess, the fact that in this work they use Pt nanoparticles as seeds for Pt nanowires growth is because this process is not totally controlled. I mean the reproducibility and the morphology and dimensions of nanowires. In fact, for me it is sufficiently explained how the authors control the Pt nanowires growth.

[ We could not image how can the reviewer #4 guess that our "process is not totally controlled". In fact, the process is so simple and easy. Liking the common CCM process used in MEA preparing for PEMFC, a matrix is made by depositing an ink on the electrolyte membrane or a decal transfer, and then grow Pt-NWs by wet chemistry. ]

Moving the electrochemical characterization, polarization curves show that in general the performance obtained with the commercial cathode is higher than those obtained with the different loadings of Pt-NPs at the cathode; particularly, in the practical range of voltage used in PEM fuel cells.

[The polarization curves of various single cells with the commercial GDE and home-made Pt-NW cathodes are shown in Fig. 3. The Pt loading ratio of the optimal Pt-NW cathode and the commercial cathode is  $0.205 \text{ mg}_{\text{Pt}} \text{ cm}^{-2}$  vs  $0.40 \text{ mg}_{\text{Pt}} \text{ cm}^{-2}$ . The home-made electrode is with about half loading of the commercial while their cell performance is similar. It is clear that the former is better than the later]

At this point it is necessary mentioning that no information was provided about the commercial gas diffusion electrode. On the other hand, the comparison should be carried out with commercial cathode with similar loading and thickness to those developed in this work.



[The commercial gas diffusion electrode was introduced in the section of experiment methods: Gas diffusion layer (GDL) (AvCarb GDS3250) and gas diffusion electrode (GDE) with Pt nanoparticle loading of  $0.40 \text{ mg cm}^{-2}$  were purchased from Ballard Power Systems and Johnson Matthey.]

[As their preparing processes and microstructures are different, the comparison between commercial cathode and the home-made one with similar loading and thickness is not suitable. For example, the optimal performance of the Pt-NW cathode is achieved at  $0.30 \text{ mg}_{\text{Pt}} \text{ cm}^{-2}$  in the Pt loading range of  $0.1 \sim 0.5 \text{ mg}_{\text{Pt}} \text{ cm}^{-2}$ , reported by our previous work (Wei Zhaoxu, *Int. J. Hydrogen Energy*, 2015, 40(7): 3068). In this paper, the Pt loading is lowered to about  $0.2 \text{ mg}_{\text{Pt}} \text{ cm}^{-2}$ ]

Regarding polarization curves showing the effect of carbon loading, the results are not consistent with those shown by impedance analysis at 0.4 V.

[Many thanks for the reviewer's carefulness. It's our mistake. In Fig 4(d), the curve symbols were corrected in the resubmitted manuscript. ]

The assessment of the catalytic activity (see Table 1) at 0.900 V requires at least previous correction of the uncompensated cell resistance, which was not performed.

[From Fig 4(a), the ohm resistances for the four samples are 0.102, 0.086, 0.084 and  $0.073 \text{ ohm cm}^{-2}$ , which correspond to 1.5, 1.6, 1.1 and 1.2 mV of the potential corrections, and their effects are neglected comparing with fuel cell experimental errors.]

The specific activity in terms of the normalization of geometric current densities by the ECSAs should be provided.

[Data of the specific current density with respect to area were added in Table 1 in the revised manuscript. ]

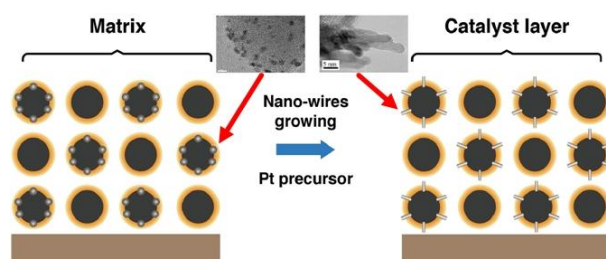
In addition, the comparison with conventional electrode has to carry out in similar conditions. Otherwise, other factors than the Pt loading and electrode thickness could affect the obtained values.

[As their preparing processes and microstructures are different, the comparison between commercial cathode and the home-made one with similar loading and thickness is not suitable. For example, the optimal performance of the Pt-NW cathode is achieved at  $0.30 \text{ mg}_{\text{Pt}} \text{ cm}^{-2}$  in the Pt loading range of  $0.1 \sim 0.5 \text{ mg}_{\text{Pt}} \text{ cm}^{-2}$ , reported by our previous work (Wei Zhaoxu, *Int. J. Hydrogen Energy*, 2015, 40(7) : 3068).]

All in all, this paper cannot be accepted for publication in International Journal of Hydrogen Energy.

Graphical abstract

Pt nanoparticles in carbon matrix enhance growth, uniformity and profile of Pt-NWs, and the Pt-NW electrodes behave high performance.



## Highlights

1. Pt nanoparticles in the carbon matrix improve uniformity and profile of Pt-NWs.
2. The novel cathode with  $0.205 \text{ mg}_{\text{Pt}} \text{ cm}^{-2}$  is comparable to commercial one.
3. A Pt-NW growth mechanism in the porous matrix is proposed.
4. This work provides a strategy for tailoring the electrode architectures.

# Pt nanowire growth induced by Pt nanoparticles in application of the cathodes for Polymer Electrolyte Membrane Fuel Cells (PEMFCs)

Sheng Sui<sup>a,b,\*</sup>, Zhaoxu Wei<sup>b</sup>, Kaihua Su<sup>b</sup>, An He<sup>b</sup>, Xiaoying Wang<sup>b</sup>, Yuehong Su<sup>a,\*</sup>, Xianghui Hou<sup>a</sup>, Saffa Raffet<sup>a</sup> and Shangfeng Du<sup>c</sup>

---

a) *Faculty of Engineering, University of Nottingham, Nottingham NG7 2RD, United Kingdom.*

b) *Institute of Fuel Cells, Shanghai Jiao Tong University, Shanghai 200240, China.*

c) *School of Chemical Engineering, University of Birmingham, Edgbaston, Birmingham B15 2TT, United Kingdom.*

## Abstract

Improving cathode performance at a lower Pt loading is critical in commercial PEMFC applications. A novel Pt nanowire (Pt-NW) cathode was developed by in-situ growth of Pt nanowires in carbon matrix consisting Pt nanoparticles (Pt-NPs). Characterization of TEM and XRD shows that the pre-existing Pt-NPs from Pt/C affect Pt-NW morphology and crystallinity and Pt profile crossing the matrix thickness. The cathode with Pt-NP loading of  $0.005 \text{ mg}_{\text{Pt-NP}} \text{ cm}^{-2}$  and total cathode Pt loading of  $0.205 \text{ mg}_{\text{Pt}} \text{ cm}^{-2}$  has the specific current density of  $89.56 \text{ A g}_{\text{Pt}}^{-1}$  at 0.9V, which is about 110 % higher than that of  $42.58 \text{ A g}_{\text{Pt}}^{-1}$  of the commercial gas diffusion layer (GDE) with Pt loading of  $0.40 \text{ mg cm}^{-2}$ . When cell voltage is below 0.48V, the Pt-NW cathode has better performance than the commercial GDE. It is believed that the excellent performance of the Pt-NW cathode is attributed to Pt-NP induction, therefore producing unique Pt-NW structure and efficient Pt utilization. A Pt-NW growth mechanism was proposed that Pt precursor diffuses into the matrix consisting of pre-existent Pt-NPs by concentration driving, and Pt-NPs provide priority sites for platinum depositing at early stage and facilitate Pt-NW growth.

## Keywords

Pt nanowire; Cathode; PEMFC; Growth; Tailoring; Architecture.

## Introduction

Hydrogen fuel cells give a choice of ultimate energy solution and attract more and more attentions in recent years. Among all kinds of fuel cells, Polymer Electrolyte Membrane Fuel Cell (PEMFC) is in the overwhelming position that is well developed and applied in the fields of vehicles, combined heat and power (CHP) systems, backup powers and power plans, etc. However, the sluggish oxygen reduction reaction (ORR) at the cathode results in a high Pt loading (currently in the range of 0.3~0.4 mg<sub>Pt</sub> cm<sup>-2</sup>) used which lead to high cost to the end users. To address this challenge, accelerating the ORR at a lower Pt loading without sacrificing performance is critical and has been pursued for decades.<sup>1,2</sup>

Until now, Pt-based electrocatalysts are practically the dominant choice in PEM fuel cells, and are mainly catalogued into the pure platinum, platinum alloys and core-shell structures.<sup>1-8</sup> To reduce expensive platinum loading and improve electrocatalytic kinetics, the ability to tailor nanostructure of electrocatalysts is critical in order to tune their geometry and electronics state.<sup>1-3,7</sup> Many fine structures, for example, Pt surface-enriched shell-core, single or multiple atom layers, multilayer alloy materials, Pt nanocage or Pt hollow, are synthesized or designed and investigated.<sup>2-10</sup> Huang et al developed a Mo-Pt<sub>3</sub>Ni/C alloy showed the best ORR performance, with a specific activity of 10.3 mA cm<sup>-2</sup> and mass activity of 6.98 A mg<sub>Pt</sub><sup>-1</sup>, which are 81- and 73-fold enhancements respectively compared with the commercial Pt/C catalyst (0.127 mA cm<sup>-2</sup> and 0.096 A mg<sub>Pt</sub><sup>-1</sup>).<sup>2</sup> A polycrystalline Pt<sub>5</sub>Pr alloy was prepared, which demonstrates ~4-fold improvement over pure Pt, comparable to that of polycrystalline Pt<sub>3</sub>Ni and many other polycrystalline Pt-alloys.<sup>4</sup> The issues for mass production arise due to the complicated processes and parameter sensibility and make them difficult in quality control in engineering, or practical applications have been limited by catalytic activity and durability.<sup>1,2</sup>

One- and two-dimensional nanomaterials with all the atoms exposed for modification act as ideal platforms for tailoring their properties and decreasing material costs.<sup>11-14</sup> The prominent characteristics of Pt nanowires (Pt-NWs) include dominant (111) facets, less lattice boundaries, a lower number of surface defect sites, and easier electron and mass transport for better electrocatalytic activity and lower vulnerability to dissolution, Ostwald ripening, and aggregation than Pt nano particles (NPs) for enhanced stability.<sup>1,12,14</sup> High Pt content catalyst (such as 70% Pt/C) is favourable for improving fuel cell performance.<sup>15</sup> Comparing with Pt nanoparticle preparing, Pt NWs can be easily prepared by template method or template-free method. Meng et al<sup>16</sup> reported factors influencing the growth of Pt Nanowires on the template-free synthesis of Pt nanowires via the chemical reduction of Pt salt precursors with formic-acid. Liang et al<sup>17</sup> used ultrathin Te@C nano cables with a very high aspect ratio as templates to form Pt@C nanocables by the galvanic replacement reaction. Kim et al<sup>18</sup> developed a nanowire network catalyst that was made of highly-dispersed Pt nanoparticles into electrospun Pt nanowire network architecture.

A new type of bimetallic nanowires (PtCo, PtNi, PtFe, etc.) have been developed by wet chemical synthesis procedure and showed high electrocatalytic activity. A bimetallic PtCo-NW/C nanostructures

possess the lowest Tafel slope, mass activity and near four-electron reduction kinetics for direct conversion of oxygen to water.<sup>19</sup> Xia et al<sup>13</sup> reported an effective solvothermal method for the direct preparation of 3D PtCo nanowire assemblies (NWAs) with tuneable composition. The mass activity of Pt<sub>59</sub>Ni<sub>41</sub> NWs is increased by a factor of 1.9 times in comparison with that of Pt NWs, and ~3.7 times with that of commercial Pt (0.09 A mgPt<sup>-1</sup>), and the higher catalytic activity and stability of Pt<sub>59</sub>Ni<sub>41</sub> NWs for the ORR is attributed as a result of the composition dependent atomic-scale alloying and faceting properties.<sup>20</sup> Recently, a new class of Pt<sub>3</sub>Fe zigzaglike nanowires (Pt-skin Pt<sub>3</sub>Fe z-NWs) with stable high-index facets (HIFs) and nanosegregated Pt-skin structure is reported. Pt-skin Pt<sub>3</sub>Fe z-NWs with a mass activity of 2.11 A mgPt<sup>-1</sup> and a specific activity of 4.34 mA cm<sup>-2</sup> for the oxygen reduction reaction (ORR) at 0.9 V versus reversible hydrogen electrode, which are the highest values in all reported PtFe-based ORR catalysts.<sup>21</sup>

For many years, the process of the nucleation and growth of nanoparticles have been depicted by the LaMer burst nucleation and following Ostwald ripening to describe the change in the particles size. Watzky and Finke formulated an approach of constant slow nucleation followed by autocatalytic growth.<sup>22</sup> Gao et al found that electrochemical deposition at a constant potential can overgrow Pt seeds, which are wet chemically synthesized Pt nanoparticles seeded homogeneously on diamond surface.<sup>23</sup> Simona et al proposed an oriented attachment growth Mechanism for silver nanowire formation.<sup>24</sup> Whatever, the nucleation and growth mechanisms behind the simple chemistry are extremely complicated.<sup>25</sup>

To boost electrocatalyst rule, optimal 3D architectures of the supports and electrodes are important to achieve efficient pt utilization and high performance in PEMFC environment as the current density of the catalyst layer is only 1/10th that if all of the transport rates are infinitely fast.<sup>26,27</sup> For constructing 3D electrode architecture, a freeze-drying/reduction process was suggested and demonstrated ultra-high pt utilization.<sup>28</sup> An aqueous suspension of GO (graphene oxide) sheets, pt precursor and nafion ionomers was spread onto a GDL, then freeze-dried and reduced while the pt precursor and go sheets were reduced to metallic pt and graphene, respectively. Novel fuel cell nanofibrous electrodes (NFEs) based on self-standing electrospun carbon nanofibre webs covered by platinum ultrathin nanoislands deposited by high overpotential pulsed electrodeposition.<sup>29</sup> These structured electrocatalyst layers have high electrical conductivity for fast charge transport and sufficient macroporosity for efficient reactant mass transportation.

Our previous work designed firstly a porous carbon matrix and grew directly pt nanowires in the pore walls of the matrix, forming a so called "Pt nanowire electrode" where the Pt nanowire morphology and distribution in the catalyst layer can be adjusted by process parameters.<sup>3,30,31</sup> The "Pt nanowire electrode" realized truly a 3D architecture as Pt-NWs growing directly on the pore wall and hence almost 100% Pt exposed to oxidant. Our further studies on effects of the matrix materials shows that, comparing with the carbon matrix, the Pt-NWs growing in a Pt/C matrix display shorter and denser fluff on the carbon support.<sup>32</sup> This reminds us that the Pt nanoparticles supported on carbon are evolved into

Pt nanowires and consequently can be favourable sites for Pt-NW growing. Following above idea, here we introduced small amount of Pt-NPs into the carbon matrix for controlling Pt-NW growth and profile, and demonstrated that the home-made electrode performance was greatly improved. Measurements of TEM, XRD, single fuel cell performance, electrochemical impedance spectrum (EIS) and cyclic voltammogram (CV) were used to characterize effects of the pre-existing Pt nanoparticles (Pt-NP) from Pt/C. Finally, a Pt-NW growing mechanism was proposed.

## Experiment methods

### Chemicals and materials

20wt% Pt/C (HiSPEC™ 3000) and 40wt% Pt/C (HiSPEC™ 4000) from Johnson Matthey; isopropanol ((CH<sub>3</sub>)<sub>2</sub>CHOH), formic acid (HCOOH), and chloroplatinic acid hexahydrate (H<sub>2</sub>PtCl<sub>6</sub> · 6H<sub>2</sub>O) from Sinopharm Chem. Reagent; commercial carbon black (Vulcan XC-72R) from Shanghai Cabot Chemical; Nafion® perfluorinated resin solution (ionomer) (DE1020, 10 wt. %) and Nafion® membrane (NR212, 50µm thickness) from DuPont. All of the above reagents and materials were used as-received without any further purification/treatment. The ultrapure water (18.2 MΩ) for preparing solution and cleaning Pt nanowires electrodes was obtained from the National Key Laboratory of Science and Technology on Micro/Nano Fabrication (NSTmnF) at Shanghai Jiao Tong University. The decal substrate was a glass-fiber contexture coated with polytetrafluoroethylene (PTFE) (ultra-premium grade) from CS Hyde Company. Gas diffusion layer (GDL) (AvCarb GDS3250) and gas diffusion electrode (GDE) with Pt nanoparticle loading of 0.40 mg cm<sup>-2</sup> were purchased from Ballard Power Systems and Johnson Matthey, respectively. High purity hydrogen (99.999%), air (99.999%) and nitrogen (99.999%) were cylinder gases.

### Pt nanowires growing promoted by Pt seeds

Similar with our previous works,<sup>32</sup> Pt-nanowires electrodes were prepared by in-situ Pt-nanowires growing in a carbon matrix, which is about 4~10µm layer of carbon powders adhered by Nafion® resin on a transfer substrate, *via* Pt persecutor reducing and then depositing in. Here, instead of pure carbon black, part of carbon black was substituted with 20wt% Pt/C, where the Pt nanoparticles serve as seeds for promoting Pt nanowires growth. Typically, a matrix ink was prepared by blending 20wt% Pt/C, commercial carbon black, Nafion® resin solution and isopropanol (Pt/C+C: ionomer=4:1, weight basis), then sonicated for 5 min. The ink was sprayed onto a decal substrate with an airbrush gun (Iwata HP-CH) at 50~60°C under an infrared light. Subsequently, the substrate was fixed on the bottom of a glass Petri dish with narrow stick tapes. 1mM chloroplatinic acid hexahydrate and formic acid solution were added to the dish in 2 hours and platinum slowly reduced, deposited and grew into Pt nanowires. After 48h, the substrate grown with Pt nanowires was taken out and rinsed for three times and immersed in deionized water for 24 hours to remove the remained ions, and then dried at 50°C for 30min. Finally, a diluted ionomer solution (0.2% by wt.) was sprayed onto the surface of the catalyst layer at an amount of 0.10



mg cm<sup>-2</sup> and dried at 50°C for 2 hours. This Pt nanowires decal was used as cathode catalyst layer in the following section.

#### **Membrane electrode assembled (MEA) fabrication and single cell polarization tests**

An anode decal was prepared with commercial Pt/C catalyst. The well mixed ink of 40 wt% Pt/C catalyst, Nafion® ionomer solution and isopropanol was sprayed onto a substrate with Pt and Nafion® ionomer loadings fixed at 0.30 and 0.10 mg cm<sup>-2</sup>, respectively. Then the anode decal was dried at 50°C for 2 hours.

A pair of the anode decal and the cathode decal were respectively placed on each side of a Nafion® NR212 electrolyte membrane and hot-pressed at 145°C for 3 mins under 0.4 MPa. After cooling to room temperature, the decal substrates were peeled off and a MEA was made. For comparison, a commercial gas diffusion electrode (GDE) with Pt loading of 0.40 mg cm<sup>-2</sup> as a cathode was used to fabricate a MEA under the same hot-pressing conditions as above.

In this paper, the deposited Pt-NW loading was fixed at 0.20 mg Pt cm<sup>-2</sup>. Pt/C (20 % Pt) loadings were varied from 0 to 0.050 mg (Pt/C) cm<sup>-2</sup> where the pre-existing Pt nano-particles are named as Pt-NPs and the Pt-NP loadings correspond to from 0 to 0.010 mg<sub>Pt-NP</sub> cm<sup>-2</sup>, while the blank carbon content fixed at 0.20 mg<sub>C</sub> cm<sup>-2</sup>. In carbon content investigation, the carbon loadings were varied with 0.10, 0.20 and 0.30 mg<sub>C</sub> cm<sup>-2</sup>, meanwhile the Pt seed loading was fixed at 0.025 mg<sub>Pt/C</sub> cm<sup>-2</sup> or 0.005 mg<sub>Pt-NP</sub> cm<sup>-2</sup>.

The MEAs with 10 cm<sup>2</sup> active area were inserted into graphite field plates with serpentine gas flow channels to assemble single cell units. The single cell units were assembled in the order of graphite field plate – sealing gasket – GDL – MEA – GDL – sealing gasket – graphite field plate, and were evaluated with an 850e Multi-Range Fuel Cell Test System (Scribner Associates Inc.). The MEAs were activated firstly with a program used in our previous work.<sup>31</sup> The temperatures of the fuel cell and two humidifiers were keeping at 70°C and 65°C, respectively. The stoichiometric ratios of hydrogen feeding and air feeding were 1.5 and 2.0, respectively. The back pressures were 1.0 bar at both sides. Polarization curves were recorded by voltage sweeping from open circuit voltage (OCV) to 0.30 V at a rate of 2 mV s<sup>-1</sup>.

#### **Characterizations**

The cross-sectional morphologies of the Pt nanowire electrodes were observed by a transmission electron microscope (TEM) (2100F, JEOL) operating at an accelerating voltage of 200 kV. The TEM samples were prepared by slicing the MEA strips embedded in the solidified epoxy resin. X-ray diffraction (XRD) patterns were recorded by a Rigaku D/max-2200/PC instrument using CuK $\alpha$  radiation ( $\lambda=1.54056$  Å) generated at 40 KV and 30 mA between 20° and 90° (2 $\theta$ ). The XRD samples of the Pt nanowires electrodes were peeled off from the MEAs. The Pt loadings of the catalyst layers were determined by inductively coupled plasma-atomic emission spectrometer (ICP-AES) (7500a, Agilent).

Cyclic voltammogram (CV) curves and electrochemical impedance spectra (EIS) spectrums were characterized in a two-electrode configuration (single cell). CV measurements on an electrochemical interface instrument (SI1287, Solartron Analytical Inc.) were recorded by voltage sweeping from 0.05 V to 1.00 V at  $25\text{mV s}^{-1}$  with 300 sccm hydrogen and 75 sccm nitrogen being supplied to the anode and cathode, respectively. The temperatures of the cell and the humidifiers were all  $35^\circ\text{C}$ . The electrochemical active surface areas (ECSAs) of Pt nanowires electrodes were calculated on the hydrogen absorption area from 0.1 to 0.4 V of the CV data, assuming that  $210\ \mu\text{C cm}^{-2}$  was needed to form a monolayer of absorbed H on polycrystalline Pt surface.<sup>34</sup> After the polarization tests, EIS tests with 885 Fuel Cell Potentiostat (Scribner Associates Inc.) were conducted at the potentials of 0.80 V and 0.40 V in a frequency range of 10 kHz~0.1 Hz with the AC amplitude of 10% DC current, and the test conditions were the same as those in the polarization measurements.

## Results and discussion

### Morphology and structure characterizations

Pt nanowires morphology was examined by TEM image analysis. To prepare TEM samples, after tested the single cells were dispatched and the MEAs were embedded in epoxy resin, and then sliced into the strips after solidified. For comparison, the TEM images in the region near the GDLs were taken up, where the Pt-NW contents were the lowest as the gradient Pt-NW distribution across the cathode thickness.<sup>31</sup> As shown in Fig. 1b, 1c, pre-existing Pt-NPs greatly improve growing uniformity of the Pt nanowires by comparing with pure carbon case in Fig. 1a. This is due to that the pre-existing Pt nanoparticles not only provide low energy interfaces for Pt nucleation, trigger the nucleation and anisotropic growth of the Pt-NPs liking Au<sup>35</sup> or Pd seeds<sup>36</sup>, but also may act as catalyst for the Pt reduction reaction. It was reported that Pd nanoparticles on the beads (a substrate) could acted as catalytic sites for the anisotropic Pt growth, and once the growth was initiated, the Pt nanowires continually grew in the  $\langle 111 \rangle$  direction until the supply of Pt<sup>0</sup> atoms was depleted.<sup>37</sup> It can be found obviously in the high-resolution TEM insets of Fig. 1(a)~(c) that with increasing the Pt nanoparticles in the carbon matrix the Pt-NWs are shorter and evenly tends unordered. This proves the existent Pt-NPs functioned as growing sites for Pt nanowires.

Fig.1

To illustrate the effect of Pt-NPs on Pt-NW crystallinity, the XRD patterns of the Pt nanowire electrodes with the Pt-NP loadings of 0, 0.005 and  $0.010\text{mg}_{\text{Pt-NP}}\text{cm}^{-2}$  were measured and shown in Fig. 2. All XRD patterns of the samples are similar with bulk platinum and Pt characteristic peaks appear at  $2\theta$  of  $39.8^\circ$ ,  $46.3^\circ$ ,  $67.5^\circ$  and  $81.6^\circ$ , respectively corresponding to the (111), (200), (220), and (311) facets. The samples at the Pt-NP loadings of 0 and  $0.005\ \text{mg}_{\text{Pt}}\text{cm}^{-2}$  have sharp and intense peaks of the (111) facet, which means perfect crystallinity and dominant (111) facets. However, more seeds liking the Pt-NP loading of  $0.010\ \text{mg cm}^{-2}$  introduce more growing sites, and lead less crystallinity or amorphous structure, which is again in well agreement with the above TEM analysis.

Fig. 2

The carbon matrix thickness, which linearly increases with carbon loadings, affected Pt nanowire distribution as Pt precursor diffuses into through the matrix micro-pores from the bulk solution. To examine Pt nanowire dispersions of various carbon loadings of 0.10, 0.20 and 0.30  $\text{mg}_C \text{cm}^{-2}$ , the TEM images near the GDLs region were photographed, where the least Pt nanowires were formed as the lowest concentrations of Pt precursor. The diffusion effect of formic acid can be ignored as it is extremely excessive ( $>100$  stoichiometric ratio). As shown in Fig. 1(d) ~ (f), the sample with the highest carbon loading of 0.30  $\text{mg}_C \text{cm}^{-2}$  has the thickest catalyst layer and the least Pt-NWs in the region near the GDE. By comparing with blank carbon as shown in Fig. 1(a), the Pt-NPs improve uniformity of Pt nanowires growing along the Pt-NW matrix thickness as depth as  $>10\mu\text{m}$  (i.e. carbon loading of 0.30  $\text{mg}_C \text{cm}^{-2}$ ).

#### Single cell performances improved by Pt nanoparticles

The polarization curves of various single cells with the commercial GDE and home-made Pt-NW cathodes are shown in Fig. 3. The Pt-NP loading of the Pt-NW cathodes is varied from 0 to 0.010  $\text{mg}_{\text{Pt-NP}} \text{cm}^{-2}$  as shown in Fig. 3(a). The optimal Pt-NP loading is obtained at 0.005  $\text{mg}_{\text{Pt-NP}} \text{cm}^{-2}$  with the current density 1.29  $\text{A cm}^{-2}$  at 0.60 V. Comparing the cell performances of the commercial GDE and the optimal Pt-NW cathode, there is a crossing point at cell voltage of 0.48 V. When the voltage is below 0.48V, the optimal Pt-NW cathode has better performance, i.e. lower concentration polarization loss, for example, its current density at 0.30 V is 7% higher than that of the commercial GDE. The lower concentration polarization is accredited to the Pt-NWs openly exposed to oxidant, not liking that in the conventional electrodes part of Pt nanoparticles lost in the dead pores or very narrow pores and cannot be accessed. On the other hand, at a higher voltage over 0.48 V, the performance of the Pt-NW cathode is slightly lower, for example, its current density at 0.60 V is about 5% lower than that of the commercial GDE. This poorer performance of the Pt-NW cathode at high voltage range may be due to its lower Pt catalyst loading,<sup>38</sup> where the Pt loading ratio of the optimal Pt-NW cathode and the commercial cathode is 0.205  $\text{mg}_{\text{Pt}} \text{cm}^{-2}$  vs 0.40  $\text{mg}_{\text{Pt}} \text{cm}^{-2}$ .

Fig. 3

EIS experiments were carried out to further evaluate the cathodes performances. Fig. 4(a) and 4(b) shows the EIS results of various Pt-NP loadings at the cell voltages of 0.80 and 0.40 V, respectively. At 0.80 V, due to the lower current density, the cathode impedances are dominated by the charge transfer resistances which are represented by the arc diameters in the Nyquist plots. The commercial GDE exhibits the smallest arc diameter, indicating the smallest charge transfer resistance and the best ORR kinetics, which corresponding to the highest current density in the high voltage range. Meanwhile, among the Pt-NW cathodes, the Pt-NW cathode with 0.005  $\text{mg}_{\text{Pt-NP}} \text{cm}^{-2}$  has the smallest charge transfer resistance, even if its Pt loading is less than that of the cathode with 0.010  $\text{mg}_{\text{Pt-NP}} \text{cm}^{-2}$ . This is due to more active (111) facets of the former supported by Fig. 2. At 0.40 V, there are two semi-circles for all samples. The high frequency arc (left) is attributed to the charge transfer impedance and double layer capacitance, and the low frequency arc (right) is related with the mass transfer resistance.<sup>39</sup> The cathode with 0.005  $\text{mg}_{\text{Pt-NP}} \text{cm}^{-2}$  has the smallest diameter of low frequency arc compared with all the other

samples, even including the commercial GDE, confirming the smallest mass transfer resistance and best performance.

Fig. 4

The Pt-NP effect on the CV curves and ECSA values of the Pt-NW cathodes are illustrated in Fig. 5(a). The ECSA value increases with the Pt-NP loading, and the maximum value of  $41.94 \text{ m}^2 \text{ g}_{\text{Pt}}^{-1}$  is achieved at a Pt-NP loading of  $0.010 \text{ mg}_{\text{Pt-NP}} \text{ cm}^{-2}$ , and the minimum value of  $36.72 \text{ m}^2 \text{ g}_{\text{Pt}}^{-1}$  at no Pt-NPs added. This trend meets with the results from TEM images in Fig. 1(a) ~ (c) and XRD patterns in Fig. 2. The increase of the ECSA value with Pt-NP loading can be attributed to the more growing/depositing sites, and therefore the Pt-NW length and the catalyst aggregation is decreased. However, at a high Pt-NP loading, such as  $0.010 \text{ mg}_{\text{Pt-NP}} \text{ cm}^{-2}$ , the excessive growing sites lead to lower Pt-NW crystallinity, presenting an indistinct crystallographic alignment as shown in the inset of Fig.1c, and finally resulting in a large charge transfer resistance and a low ORR activity.

Fig. 5

#### Effects of matrix carbon loadings on single cell performance

The carbon loading in the matrix determines the cathode thickness, and there is a linear relationship between them.<sup>40</sup> There is a balance between the mass transfer resistance and Pt-NW aggregation. Performance curves of the Pt-NW cathodes with different carbon loadings are shown in Fig. 3(b). The performance curves of the Pt-NW cathode with  $0.10 \text{ mg}_C \text{ cm}^{-2}$  and  $0.20 \text{ mg}_C \text{ cm}^{-2}$  are quite similar, for example, their current densities at  $0.60 \text{ V}$  are about  $1.35 \text{ A cm}^{-2}$ . Among the Pt-NW cathodes, the  $0.10 \text{ mg}_C \text{ cm}^{-2}$  one is the highest power density at the cell voltage  $> 0.53 \text{ V}$ , while the  $0.20 \text{ mg}_C \text{ cm}^{-2}$  one the best at the cell voltage  $< 0.53 \text{ V}$ . The Pt-NW cathode with  $0.30 \text{ mg}_C \text{ cm}^{-2}$  exhibits the poorest performance, which means that the thick cathode causes deleterious mass transfer polarization.

The EIS results of the Pt-NW cathodes with different carbon loadings are illustrated in Fig. 4(c) and 4(d). It can be seen that, the cathode with  $0.10 \text{ mg}_C \text{ cm}^{-2}$  has the smallest impedance at  $0.80 \text{ V}$  while one with  $0.3 \text{ mg}_C \text{ cm}^{-2}$  has the largest impedance at  $0.40 \text{ V}$ , suggesting their smallest charge transfer resistance and the largest mass transfer resistance, respectively. The cathode with  $0.20 \text{ mg}_C \text{ cm}^{-2}$  exhibits the smallest mass transfer resistance at  $0.40 \text{ V}$ . Hence, the  $0.20 \text{ mg}_C \text{ cm}^{-2}$  one has an optimal performance at low voltage range.

To further investigate the effect of carbon contents, the cycle voltammograms were recorded to evaluate the electrode ECSAs, and the results are presented in Fig. 5(b). The maximum ECSA value is  $58.06 \text{ m}^2 \text{ g}_{\text{Pt}}^{-1}$  obtained at  $0.10 \text{ mg}_C \text{ cm}^{-2}$ , and drops to  $27.85 \text{ m}^2 \text{ g}_{\text{Pt}}^{-1}$  when the carbon loading is  $0.30 \text{ mg}_C \text{ cm}^{-2}$ . This can reason that the ionomer sprayed cannot reach on the deep Pt-NWs which could not contribute to electrochemistry. The value of  $58.06 \text{ m}^2 \text{ g}_{\text{Pt}}^{-1}$  is even higher than that of  $47.0 \text{ m}^2 \text{ g}_{\text{Pt}}^{-1}$  of the conventional Pt/C electrode reported in our previous work.<sup>30</sup> However, except of ECSA, the cathode reaction also depends on conductivity and oxygen supplying. Therefore, the optimal carbon loading is  $0.20 \text{ mg}_C \text{ cm}^{-2}$ .

#### Pt efficiency comparing

Catalyst activity measurements of MEAs are generally evaluated using H<sub>2</sub>/O<sub>2</sub> reactants in order to minimize mass transport resistances.<sup>41</sup> To comparing Pt efficiency under real H<sub>2</sub>/air operating conditions, here the current density data at 0.9 V were taken and the specific current densities (SCDs) on Pt mass basis were calculated according to the data from Fig. 3(a). The SCDs of the home-made Pt-NW cathodes with Pt seeds loadings of 0, 0.005, and 0.010 mg<sub>Pt-NP</sub> cm<sup>-2</sup> and the commercial GDE are summarized in Table 1. The Pt-NW cathode with 0.005 mg<sub>Pt-NP</sub> cm<sup>-2</sup> has the highest SCD value of 89.56 A g<sub>Pt</sub><sup>-1</sup>, which is 47 % higher than 60.95 A g<sub>Pt</sub><sup>-1</sup> of the 0.010 mg<sub>Pt-NP</sub> cm<sup>-2</sup> one and 110% higher than 42.58 A g<sub>Pt</sub><sup>-1</sup> of the commercial GDE. The 0.005 mg<sub>Pt-NP</sub> cm<sup>-2</sup> one has the optimal catalyst utilization, although its ECSA value is a little smaller than that of the 0.010 mg<sub>Pt-NP</sub> cm<sup>-2</sup> sample. The SCD value of the commercial GDE is the smallest, and is less half of the 0.005 mg Pt-NP cm<sup>-2</sup> sample. The high Pt efficiency of the Pt-NW cathodes is according to: i) Pt-NWs grow directly on the pore wall almost with no hiding; ii) P-NP seeds induce uniform growing of Pt-NWs; and iii) dominant (111) facets with high catalytic activity for oxygen reduction reaction (ORR).

Table 1

#### **Mechanism of Pt nanowires growing on Pt nanoparticle seeds**

There are many mechanisms of nucleation and growth in solutions such as LaMer nucleation, Finke-Watzky two step mechanism, Ostwald ripening, digestive ripening, coalescence and orientated attachment, and intra-particle growth.<sup>28</sup> However, these mechanisms are in conflicts or inverse with some others, for example, the nucleation and growth could occur simultaneously by Finke-Watzky mechanism or separately by LaMer mechanism. Cheong et al<sup>42</sup> investigated the precursor concentrations effects by in situ and ex situ methods and found the low concentration growth occurs at a relatively slow rate and yields faceted morphologies, are characteristic of a thermodynamically controlled regime. It is thought that incomplete reduction of AuCl precursor allows only a part of it to transform to Au, which can seed nanowire growth.<sup>43</sup> Meng et al<sup>16</sup> demonstrated that both formate as the intermediate species and HCOOH in the reacting solution (PH=1.5~3.5) are significantly important, while formate reduces the Pt salt and HCOOH block all Pt surfaces except Pt (111) facets.

The catalytic phenomena of Pt-NP seeds was observed obviously in present experimental. When Pt-NPs (supported on carbon) added in the matrix, the color of the solution containing Pt precursor fades from light yellow to colorless in less than 12hrs, comparing that more than 24hrs without Pt-NPs. The proposed schematic of Pt nanowires growth mechanism in the carbon matrix is illustrated in Fig. 6. It is assumed that the platinum precursors and formic acid diffuse into the the matrix consisting of carbon powders and Pt-NPs bonded by ionomer. Then the Pt seeds facilitate platinum precursor reduction and provide depositing sites for the newly formed Pt atoms which are nearly layer-by-layer monomer addition onto the crystallite faces to yield stable morphology. Except of reducing function, overwhelming formic acid also serves for capping agent, therefore platinum atoms add onto the (111) facet and the sole nanowire morphology were produced. Concentration difference of platinum precursor, driving from the bulk into the matrix through the micro pores, leads to a gradient Pt-NW profile. Nanocrystal growth

in the low concentration reaction, here 1mM chloroplatinic acid hexahydrate adopted, occurs under thermodynamic control.<sup>42</sup> Here weak reducing agent, low concentrations of the reactants and low temperature ensure a slow reaction rate. Formic acid as capping agent plays an important role and promotes an anisotropy growth along (111) facets.<sup>16</sup> On the other hand, catalytic and seed functions of Pt-NPs induce Pt atoms deposited preferentially on the Pt-NPs, not carbon particles, and result in relatively progressive gradient or better uniformity along the matrix thickness. It was evidenced by the results of the TEM images and XRD patterns as shown in Fig. 1(a)~(c) and Fig. 2, where the more Pt-NP seeds, the shorter nanowires at the same Pt depositing amount.

Fig. 6

## Conclusions

In summary, a novel Pt-NW cathode with low Pt loading was developed by introducing Pt nanoparticles (Pt-NPs) into a carbon matrix and in-situ growing Pt nanowires. The pre-existing Pt nanoparticles provide low energy interfaces for Pt nucleation and thus induce the Pt nanowire growth, therefore avoid the Pt nanowire aggregation. However, excessive Pt nanoparticles decrease length and crystallinity of the Pt nanowires, even if resulting in an amorphous structure. The carbon loading in the matrix dominates the matrix thickness and Pt profile. The optimal Pt-NW cathode is with Pt-NP loading of  $0.005 \text{ mg}_{\text{Pt-NP}} \text{ cm}^{-2}$  and carbon loading of  $0.02 \text{ mg}_{\text{C}} \text{ cm}^{-2}$ , respectively. The optimal cathode with total cathode Pt loading of  $0.205 \text{ mg cm}^{-2}$  has the highest specific current density of  $89.56 \text{ A g}_{\text{Pt}}^{-1}$  at 0.9V under air/H<sub>2</sub> feeding, which is about 110% higher than that of the commercial GDE with Pt loading of  $0.40 \text{ mg cm}^{-2}$ . When the cell voltage is below 0.48V, the optimal Pt-NW cathode has better performance than the commercial GDE. Good performance of the Pt-NW cathodes was attributed to i) uniform Pt-NW growth induced by Pt-NPs; ii) high Pt utilization as Pt-NWs growing directly on the pore wall and hence fully exposed to oxidant iii) dominant (111) facets of the Pt-NWs with high ORR catalytic activity. A Pt-NW growth mechanism was proposed that Pt precursor diffuses into the matrix of pre-existing Pt-NPs by concentration driving, and Pt-NPs as seeds induce Pt-NW growth kinetics and provide priority sites for platinum depositing. This work provides a new strategy for tailoring Pt-NW nanostructures and designing the electrode architectures, and can be extended to the other electrocatalysts of alloys or alloying nanowires.

## Acknowledgements

We gratefully acknowledge the financial supports from the *European Union's Horizon 2020 research and innovation programme H2020-MSCA-IF-2014* under grant agreement No 658217, *the National Natural Science Foundation of China* under grant agreement No 21576164, and *the International Science & Technology Cooperation Program of the Ministry of Science & Technology* (grant No. 2015DFG62250).

## references

- 1 Ifan Erfyl Lester Stephens, Jan Rossmeisl and Ib Chorkendorff, *Science*, 2016, 354 (6318), 1378.
- 2 Xiaoqing Huang, Zipeng Zhao, Liang Cao, Yu Chen, Enbo Zhu, Zhaoyang Lin, Mufan Li, Aiming Yan, Alex Zettl, Y. Morris Wang, Xiangfeng Duan, Tim Mueller and Yu Huang, *Science*, 2015, 348(6240), 1230.
- 3 Sheng Sui, Xiaoying Wang, Xintong Zhou, Yuehong Su, Saffa B Riffat and Chang-jun Liu, *J. Mater. Chem. A*, 2017, 5, 1808.
- 4 Batyr Garlyyev, Marcus D Pohl, Viktor Čolić, Yunchang Liang, Faheem K Butt, Alexander Holleitner, and Aliaksandr S Bandarenka, *Electrochem. Commun.*, 2018, 88, 10.
- 5 NamgeeJung, Dong YoungChung, JaeyuneRyu, Sung JongYoo and Yung-EunSung, *Nano Today*, 2014, 9, 433.
- 6 Laetitia Dubau, Miguel Lopez-Haro, Julien Durst, Laure Guétaz, Pascale Bayle-Guillemaud, Marian Chatenetab and Frédéric Maillard, *J. Mater. Chem. A*, 2014, 2, 18497
- 7 Yijin Kang, Peidong Yang, Nenad M. Markovic and Vojislav R. Stamenkovic, *Nano Today*, 2016, 11, 587.
- 8 María Escudero-Escribano, Paolo Malacrida, Martin H. Hansen, Ulrik G. Vej-Hansen, Amado Velázquez-Palenzuela, Vladimir Tripkovic, Jakob Schiøtz, Jan Rossmeisl, Ifan E. L. Stephens and Ib Chorkendorff, *Science*, 2016, 352(6281), 73.
- 9 Tim Van Cleve, Saman Moniri, Gabrielle Belok, Karren L. More and Suljo Linic, *ACS Catal.*, 2017, 7, 17.
- 10 Arup Mahata, Kuber Singh Rawat, Indrani Choudhuri and Biswarup Pathak, *J. Mater. Chem. A*, 2016, 4, 12756.
- 11 Muhammad Aurang Zeb Gul Sial, Muhammad Aizaz Ud Din and Xun Wang, *Chem. Soc. Rev.*, 2018, DOI: 10.1039/c8cs00113h
- 12 Wei Wang, Fan Lv, Bo Lei, Sheng Wan, Mingchuan Luo and Shaojun Guo, *Adv. Mater.*, 2016, 28, 10117.
- 13 BY Xia, HB Wu, N Li, Y Yan, XW Lou and X Wang, *Angew. Chem. Int. Ed.*, 2015, 54(12), 3797.
- 14 Yaxiang Lu, Shangfeng Du and Robert Steinberger-Wilckens, *Appl. Catal. B: Environ.*, 2016, 199, 292.
- 15 Yameng Wang, Liangliang Zou, Qinghong Huang, Zhiqing Zou and Hui Yang, *Int. J. Hydrogen Energy*, 2017, 42(43), 26695.
- 16 Hui Meng , Yunfeng Zhan , Dongrong Zeng , Xiaoxue Zhang , Guoqing Zhang and Frédéric Jaouen, *small*, 2015, 11(27), 3377.
- 17 Hai-Wei Liang, Xiang Cao, Fei Zhou, Chun-Hua Cui, Wen-Jun Zhang and Shu-Hong Yu, *Adv. Mater.*, 2011, 23, 1467.
- 18 HJ Kim, YS Kim, MH Seo, SM Choi, J Cho, GW Huber and WB Kim, *Electrochem. Commun.*, 2010,12(1), 32.
- 19 Robert Wainright and Ramaraja P. Ramasamy, *J. Electrochem. Soc.*, 2016, 163 (6), F533.
- 20 Fangfang Chang, Gang Yu, Shiyao Shan, Zakiya Skeete, Jinfang Wu, Jin Luo, Yang Ren, Valeri Petkov and Chuan-Jian Zhong, *J. Mater. Chem. A*, 2017, 5, 12557.
- 21 Mingchuan Luo, Yingjun Sun, Xu Zhang, Yingnan Qin, Mingqiang Li, Yingjie Li, Chunji Li, Yong Yang, Lei Wang, Peng Gao, Gang Lu and Shaojun Guo, *Adv. Mater.*, 2018, 30, 1705515
- 22 T. Nguyen, K. Thanh, N. Maclean and S. Mahiddine, *Chem. Rev.*, 2014, 114, 7610
- 23 Fang Gao, Nianjun Yang, Waldemar Smirnov, Harald Obloh and Christoph E. Nebel, *Electrochim. Acta*, 2013, 90, 445.

- 24 Simona E. Hunyadi Murph, Catherine J. Murphy, Austin Leach and Kenneth Gall, *Cryst. Growth Des.*, 2015, 15, 1968.
- 25 Younan Xia, Yujie Xiong, Byungkwon Lim and Sara E. Skrabalak, *Angew. Chem. Int. Ed.*, 2008, 47, 2.
- 26 S. Litster, W. K. Epting, E. A. Wargo, S. R. Kalidindi and E. C. Kumbur, *Fuel Cells*, 2013, 13(5), 935.
- 27 Gokce S. Avcioglu, Berker Ficicilar and Inci Eroglu, *Int. J. Hydrogen Energy*, 2018, 43(23), 10779.
- 28 Zhangxun Xia, Suli Wang, Luhua Jiang, Hai Sun, Fulai Qi, Jutao Jin, Gongquan Sun, *J. Mater. Chem. A*, 2015, 3, 1641.
- 29 Giorgio Ercolano, Filippo Farina, Sara Cavaliere, Deborah J. Jones and Jacques Rozière, *J. Mater. Chem. A*, 2017, 5, 3974
- 30 Xianyong Yao, Kaihua Su, Sheng Sui, Liwei Mao, An He, Junliang Zhang and Shangfeng Du, *Int. J. Hydrogen Energy*, 2013, 38(28), 12374.
- 31 Zhaoxu Wei, An He, Kaihua Su, Sheng Sui, *J. Energy Chem.*, 2015, 24(2), 213.
- 32 K Su, X Yao, S Sui, Z Wei, J Zhang and S Du, *Fuel Cells*, 2015, 15(3), 449.
- 33 Xuhai Wang, Francis W. Richey, Kevin H. Wujcik and Yossef A. Elabd, *J. Power Sources*, 2014, 264, 42.
- 34 Zheng Fang, Yuliang Zhang, Feifei Du and Xinhua Zhong, *Nano. Res.*, 2008, 1, 249.
- 35 Gilles Berhault, Marta Bausach, Laure Bisson, Loïc Becerra, Cécile Thomazeau and Denis Uzio, *J. Phys. Chem. C*, 2007, 111, 5915.
- 36 Eric P. Lee, Jingyi Chen, Yadong Yin, Charles T. Campbell and Younan Xia, *Adv. Mater.*, 2006, 18, 3271.
- 37 S Du and BG Pollet, *Int. J. Hydrogen Energy*, 2012, 37, 17892.
- 38 Mariana Ciureanu and Raymond Roberge, *J. Phys. Chem. B*, 2001, 105, 3531.
- 39 Kaihua Su, Sheng Sui, Xianyong Yao, Zhaoxu Wei, Junliang Zhang and Shangfeng Du, *Int. J. Hydrogen Energy*, 2014, 39, 3397.
- 40 Hubert A. Gasteiger, Shyam S. Kocha, Bhaskar Sompalli and Frederick T. Wagner, *Appl. Catal. B: Environ.*, 2005, 56, 9.
- 41 Hubert A. Gasteiger, Shyam S. Kocha, Bhaskar Sompalli and Frederick T. Wagner, *Appl. Catal. B: Environ.*, 2005, 56, 9.
- 42 Soshan Cheong, John Watt, Bridget Ingham, Michael F. Toney and Richard D. Tilley, *J. Am. Chem. Soc.*, 2009, 131, 14590.
- 43 Paromita Kundu, Aditi Halder, B. Viswanath, Dipan Kundu, Ganpati Ramanath and N. Ravishankar, *J. Am. Chem. Soc.*, 2010, 132, 20.



# Pt nanowire growth induced by Pt nanoparticles in application of the cathodes for Polymer Electrolyte Membrane Fuel Cells (PEMFCs)

Sheng Sui<sup>a,b,\*</sup>, Zhaoxu Wei<sup>b</sup>, Kaihua Su<sup>b</sup>, An He<sup>b</sup>, Xiaoying Wang<sup>b</sup>, Yuehong Su<sup>a,\*</sup>, Xianghui Hou<sup>a</sup>, Saffa Raffet<sup>a</sup> and Shangfeng Du<sup>c</sup>

---

a) *Faculty of Engineering, University of Nottingham, Nottingham NG7 2RD, United Kingdom.*

b) *Institute of Fuel Cells, Shanghai Jiao Tong University, Shanghai 200240, China.*

c) *School of Chemical Engineering, University of Birmingham, Edgbaston, Birmingham B15 2TT, United Kingdom.*

## Abstract

Improving cathode performance at a lower Pt loading is critical in commercial PEMFC applications. A novel Pt nanowire (Pt-NW) cathode was developed by in-situ growth of Pt nanowires in carbon matrix consisting Pt nanoparticles (Pt-NPs). Characterization of TEM and XRD shows that the pre-existing Pt-NPs from Pt/C affect Pt-NW morphology and crystallinity and Pt profile **crossing** the matrix thickness. The cathode with Pt-NP loading of  $0.005 \text{ mg}_{\text{Pt-NP}} \text{ cm}^{-2}$  and total cathode Pt loading of  $0.205 \text{ mg}_{\text{Pt}} \text{ cm}^{-2}$  has the specific current density of  $89.56 \text{ A g}_{\text{Pt}}^{-1}$  at 0.9V, which is about 110 % higher than that of  $42.58 \text{ A g}_{\text{Pt}}^{-1}$  of the commercial gas diffusion layer (GDE) with Pt loading of  $0.40 \text{ mg cm}^{-2}$ . When cell voltage is below 0.48V, the Pt-NW cathode has better performance than the commercial GDE. It is believed that the excellent performance of the Pt-NW cathode is attributed to Pt-NP induction, therefore producing unique Pt-NW structure and **efficient** Pt utilization. A Pt-NW growth mechanism was proposed that Pt precursor diffuses into the matrix consisting of pre-existent Pt-NPs by concentration driving, and Pt-NPs provide priority sites for platinum depositing at early stage and facilitate Pt-NW growth.

Keywords

Pt nanowire; Cathode; PEMFC; Growth; Tailoring; Architecture.

## Introduction

Hydrogen fuel cells give a choice of ultimate energy solution and attract more and more attentions in recent years. Among all kinds of fuel cells, Polymer Electrolyte Membrane Fuel Cell (PEMFC) is in the overwhelming position that is well developed and applied in the fields of vehicles, combined heat and power (CHP) systems, backup powers and power plants, etc. However, the sluggish oxygen reduction reaction (ORR) at the cathode results in a high Pt loading (currently in the range of 0.3~0.4 mg<sub>Pt</sub> cm<sup>-2</sup>) used which lead to high cost to the end users. To address this challenge, accelerating the ORR at a lower Pt loading without sacrificing performance is critical and has been pursued for decades.<sup>1,2</sup>

Until now, Pt-based electrocatalysts are practically the dominant choice in PEM fuel cells, and are mainly catalogued into the pure platinum, platinum alloys and core-shell structures.<sup>1-8</sup> To reduce expensive platinum loading and improve electrocatalytic kinetics, the ability to tailor nanostructure of electrocatalysts is critical in order to tune their geometry and electronics state.<sup>1-3,7</sup> Many fine structures, for example, Pt surface-enriched shell-core, single or multiple atom layers, multilayer alloy materials, Pt nanocage or Pt hollow, are synthesized or designed and investigated.<sup>2-10</sup> Huang et al developed a Mo-Pt<sub>3</sub>Ni/C alloy showed the best ORR performance, with a specific activity of 10.3 mA cm<sup>-2</sup> and mass activity of 6.98 A mg<sub>Pt</sub><sup>-1</sup>, which are 81- and 73-fold enhancements respectively compared with the commercial Pt/C catalyst (0.127 mA cm<sup>-2</sup> and 0.096 A mg<sub>Pt</sub><sup>-1</sup>).<sup>2</sup> A polycrystalline Pt<sub>5</sub>Pr alloy was prepared, which demonstrates ~4-fold improvement over pure Pt, comparable to that of polycrystalline Pt<sub>3</sub>Ni and many other polycrystalline Pt-alloys.<sup>4</sup> The issues for mass production arise due to the complicated processes and parameter sensibility and make them difficult in quality control in engineering, or practical applications have been limited by catalytic activity and durability.<sup>1,2</sup>

One- and two-dimensional nanomaterials with all the atoms exposed for modification act as ideal platforms for tailoring their properties and decreasing material costs.<sup>11-14</sup> The prominent characteristics of Pt nanowires (Pt-NWs) include dominant (111) facets, less lattice boundaries, a lower number of surface defect sites, and easier electron and mass transport for better electrocatalytic activity and lower vulnerability to dissolution, Ostwald ripening, and aggregation than Pt nano particles (NPs) for enhanced stability.<sup>1,12,14</sup> High Pt content catalyst (such as 70% Pt/C) is favourable for improving fuel cell performance.<sup>15</sup> Comparing with Pt nanoparticle preparing, Pt NWs can be easily prepared by template method or template-free method. Meng et al<sup>16</sup> reported factors influencing the growth of Pt Nanowires on the template-free synthesis of Pt nanowires via the chemical reduction of Pt salt precursors with formic-acid. Liang et al<sup>17</sup> used ultrathin Te@C nano cables with a very high aspect ratio as templates to form Pt@C nanocables by the galvanic replacement reaction. Kim et al<sup>18</sup> developed a nanowire network catalyst that was made of highly-dispersed Pt nanoparticles into electrospun Pt nanowire network architecture.

A new type of bimetallic nanowires (PtCo, PtNi, PtFe, etc.) have been developed by wet chemical synthesis procedure and showed high electrocatalytic activity. A bimetallic PtCo-NW/C nanostructures

possess the lowest Tafel slope, mass activity and near four-electron reduction kinetics for direct conversion of oxygen to water.<sup>19</sup> Xia et al<sup>13</sup> reported an effective solvothermal method for the direct preparation of 3D PtCo nanowire assemblies (NWAs) with tuneable composition. The mass activity of Pt<sub>59</sub>Ni<sub>41</sub> NWs is increased by a factor of 1.9 times in comparison with that of Pt NWs, and ~3.7 times with that of commercial Pt (0.09 A mgPt<sup>-1</sup>), and the higher catalytic activity and stability of Pt<sub>59</sub>Ni<sub>41</sub> NWs for the ORR is attributed as a result of the composition dependent atomic-scale alloying and faceting properties.<sup>20</sup> Recently, a new class of Pt<sub>3</sub>Fe zigzaglike nanowires (Pt-skin Pt<sub>3</sub>Fe z-NWs) with stable high-index facets (HIFs) and nanosegregated Pt-skin structure is reported. Pt-skin Pt<sub>3</sub>Fe z-NWs with a mass activity of 2.11 A mgPt<sup>-1</sup> and a specific activity of 4.34 mA cm<sup>-2</sup> for the oxygen reduction reaction (ORR) at 0.9 V versus reversible hydrogen electrode, which are the highest values in all reported PtFe-based ORR catalysts.<sup>21</sup>

For many years, the process of the nucleation and growth of nanoparticles have been depicted by the LaMer burst nucleation and following Ostwald ripening to describe the change in the particles size. Watzky and Finke formulated an approach of constant slow nucleation followed by autocatalytic growth.<sup>22</sup> Gao et al found that electrochemical deposition at a constant potential can overgrow Pt seeds, which are wet chemically synthesized Pt nanoparticles seeded homogeneously on diamond surface.<sup>23</sup> Simona et al proposed an oriented attachment growth Mechanism for silver nanowire formation.<sup>24</sup> Whatever, the nucleation and growth mechanisms behind the simple chemistry are extremely complicated.<sup>25</sup>

To boost electrocatalyst rule, optimal 3D architectures of the supports and electrodes are important to achieve efficient pt utilization and high performance in PEMFC environment as the current density of the catalyst layer is only 1/10th that if all of the transport rates are infinitely fast.<sup>26,27</sup> For constructing 3D electrode architecture, a freeze-drying/reduction process was suggested and demonstrated ultra-high pt utilization.<sup>28</sup> An aqueous suspension of GO (graphene oxide) sheets, pt precursor and nafion ionomers was spread onto a GDL, then freeze-dried and reduced while the pt precursor and go sheets were reduced to metallic pt and graphene, respectively. Novel fuel cell nanofibrous electrodes (NFEs) based on self-standing electrospun carbon nanofibre webs covered by platinum ultrathin nanoislands deposited by high overpotential pulsed electrodeposition.<sup>29</sup> These structured electrocatalyst layers have high electrical conductivity for fast charge transport and sufficient macroporosity for efficient reactant mass transportation.

Our previous work designed firstly a porous carbon matrix and grew directly pt nanowires in the pore walls of the matrix, forming a so called “Pt nanowire electrode” where the Pt nanowire morphology and distribution in the catalyst layer can be adjusted by process parameters.<sup>3,30,31</sup> The “Pt nanowire electrode” realized truly a 3D architecture as Pt-NWs growing directly on the pore wall and hence almost 100% Pt exposed to oxidant. Our further studies on effects of the matrix materials shows that, comparing with the carbon matrix, the Pt-NWs growing in a Pt/C matrix display shorter and denser fluff on the carbon support.<sup>32</sup> This reminds us that the Pt nanoparticles supported on carbon are evolved into

Pt nanowires and consequently can be favourable sites for Pt-NW growing. Following above idea, here we introduced small amount of Pt-NPs into the carbon matrix for controlling Pt-NW growth and profile, and demonstrated that the home-made electrode performance was greatly improved. Measurements of TEM, XRD, single fuel cell performance, electrochemical impedance spectrum (EIS) and cyclic voltammogram (CV) were used to characterize effects of the pre-existing Pt nanoparticles (Pt-NP) from Pt/C. Finally, a Pt-NW growing mechanism was proposed.

## Experiment methods

### Chemicals and materials

20wt% Pt/C (HiSPEC™ 3000) and 40wt% Pt/C (HiSPEC™ 4000) from Johnson Matthey; isopropanol ((CH<sub>3</sub>)<sub>2</sub>CHOH), formic acid (HCOOH), and chloroplatinic acid hexahydrate (H<sub>2</sub>PtCl<sub>6</sub> · 6H<sub>2</sub>O) from Sinopharm Chem. Reagent; commercial carbon black (Vulcan XC-72R) from Shanghai Cabot Chemical; Nafion® perfluorinated resin solution (ionomer) (DE1020, 10 wt. %) and Nafion® membrane (NR212, 50µm thickness) from DuPont. All of the above reagents and materials were used as-received without any further purification/treatment. The ultrapure water (18.2 MΩ) for preparing solution and cleaning Pt nanowires electrodes was obtained from the National Key Laboratory of Science and Technology on Micro/Nano Fabrication (NSTmnF) at Shanghai Jiao Tong University. The decal substrate was a glass-fiber contexture coated with polytetrafluoroethylene (PTFE) (ultra-premium grade) from CS Hyde Company. Gas diffusion layer (GDL) (AvCarb GDS3250) and gas diffusion electrode (GDE) with Pt nanoparticle loading of 0.40 mg cm<sup>-2</sup> were purchased from Ballard Power Systems and Johnson Matthey, respectively. High purity hydrogen (99.999%), air (99.999%) and nitrogen (99.999%) were cylinder gases.

### Pt nanowires growing promoted by Pt seeds

Similar with our previous works,<sup>32</sup> Pt-nanowires electrodes were prepared by in-situ Pt-nanowires growing in a carbon matrix, which is about 4~10µm layer of carbon powders adhered by Nafion® resin on a transfer substrate, *via* Pt persecutor reducing and then depositing in. Here, instead of pure carbon black, part of carbon black was substituted with 20wt% Pt/C, where the Pt nanoparticles serve as seeds for promoting Pt nanowires growth. Typically, a matrix ink was prepared by blending 20wt% Pt/C, commercial carbon black, Nafion® resin solution and isopropanol (Pt/C+C: ionomer=4:1, weight basis), then sonicated for 5 min. The ink was sprayed onto a decal substrate with an airbrush gun (Iwata HP-CH) at 50~60°C under an infrared light. Subsequently, the substrate was fixed on the bottom of a glass Petri dish with narrow stick tapes. 1mM chloroplatinic acid hexahydrate and formic acid solution were added to the dish in 2 hours and platinum slowly reduced, deposited and grew into Pt nanowires. After 48h, the substrate grown with Pt nanowires was taken out and rinsed for three times and immersed in deionized water for 24 hours to remove the remained ions, and then dried at 50°C for 30min. Finally, a diluted ionomer solution (0.2% by wt.) was sprayed onto the surface of the catalyst layer at an amount of 0.10

mg cm<sup>-2</sup> and dried at 50°C for 2 hours. This Pt nanowires decal was used as cathode catalyst layer in the following section.

#### **Membrane electrode assembled (MEA) fabrication and single cell polarization tests**

An anode decal was prepared with commercial Pt/C catalyst. The well mixed ink of 40 wt% Pt/C catalyst, Nafion® ionomer solution and isopropanol was sprayed onto a substrate with Pt and Nafion® ionomer loadings fixed at 0.30 and 0.10 mg cm<sup>-2</sup>, respectively. Then the anode decal was dried at 50°C for 2 hours.

A pair of the anode decal and the cathode decal were respectively placed on each side of a Nafion® NR212 electrolyte membrane and hot-pressed at 145°C for 3 mins under 0.4 MPa. After cooling to room temperature, the decal substrates were peeled off and a MEA was made. For comparison, a commercial gas diffusion electrode (GDE) with Pt loading of 0.40 mg cm<sup>-2</sup> as a cathode was used to fabricate a MEA under the same hot-pressing conditions as above.

In this paper, the deposited Pt-NW loading was fixed at 0.20 mg Pt cm<sup>-2</sup>. Pt/C (20 % Pt) loadings were varied from 0 to 0.050 mg (Pt/C) cm<sup>-2</sup> where the pre-existing Pt nano-particles are named as Pt-NPs and the Pt-NP loadings correspond to from 0 to 0.010 mg<sub>Pt-NP</sub> cm<sup>-2</sup>, while the blank carbon content fixed at 0.20 mg<sub>C</sub> cm<sup>-2</sup>. In carbon content investigation, the carbon loadings were varied with 0.10, 0.20 and 0.30 mg<sub>C</sub> cm<sup>-2</sup>, meanwhile the Pt seed loading was fixed at 0.025 mg<sub>Pt/C</sub> cm<sup>-2</sup> or 0.005 mg<sub>Pt-NP</sub> cm<sup>-2</sup>.

The MEAs with 10 cm<sup>2</sup> active area were inserted into graphite field plates with serpentine gas flow channels to assemble single cell units. The single cell units were assembled in the order of graphite field plate – sealing gasket – GDL – MEA – GDL – sealing gasket – graphite field plate, and were evaluated with an 850e Multi-Range Fuel Cell Test System (Scribner Associates Inc.). The MEAs were activated firstly with a program used in our previous work.<sup>31</sup> The temperatures of the fuel cell and two humidifiers were keeping at 70°C and 65°C, respectively. The stoichiometric ratios of hydrogen feeding and air feeding were 1.5 and 2.0, respectively. The back pressures were 1.0 bar at both sides. Polarization curves were recorded by voltage sweeping from open circuit voltage (OCV) to 0.30 V at a rate of 2 mV s<sup>-1</sup>.

#### **Characterizations**

The cross-sectional morphologies of the Pt nanowire electrodes were observed by a transmission electron microscope (TEM) (2100F, JEOL) operating at an accelerating voltage of 200 kV. The TEM samples were prepared by slicing the MEA strips embedded in the solidified epoxy resin. X-ray diffraction (XRD) patterns were recorded by a Rigaku D/max-2200/PC instrument using CuK $\alpha$  radiation ( $\lambda=1.54056$  Å) generated at 40 KV and 30 mA between 20° and 90° (2 $\theta$ ). The XRD samples of the Pt nanowires electrodes were peeled off from the MEAs. The Pt loadings of the catalyst layers were determined by inductively coupled plasma-atomic emission spectrometer (ICP-AES) (7500a, Agilent).

Cyclic voltammogram (CV) curves and electrochemical impedance spectra (EIS) spectrums were characterized in a two-electrode configuration (single cell). CV measurements on an electrochemical interface instrument (SI1287, Solartron Analytical Inc.) were recorded by voltage sweeping from 0.05 V to 1.00 V at  $25\text{mV s}^{-1}$  with 300 sccm hydrogen and 75 sccm nitrogen being supplied to the anode and cathode, respectively. The temperatures of the cell and the humidifiers were all  $35^\circ\text{C}$ . The electrochemical active surface areas (ECSAs) of Pt nanowires electrodes were calculated on the hydrogen absorption area from 0.1 to 0.4 V of the CV data, assuming that  $210\ \mu\text{C cm}^{-2}$  was needed to form a monolayer of absorbed H on polycrystalline Pt surface.<sup>34</sup> After the polarization tests, EIS tests with 885 Fuel Cell Potentiostat (Scribner Associates Inc.) were conducted at the potentials of 0.80 V and 0.40 V in a frequency range of 10 kHz~0.1 Hz with the AC amplitude of 10% DC current, and the test conditions were the same as those in the polarization measurements.

## Results and discussion

### Morphology and structure characterizations

Pt nanowires morphology was examined by TEM image analysis. To prepare TEM samples, after tested the single cells were dispatched and the MEAs were embedded in epoxy resin, and then sliced into the strips after solidified. For comparison, the TEM images in the region near the GDLs were taken up, where the Pt-NW contents were the lowest as the gradient Pt-NW distribution across the cathode thickness.<sup>31</sup> As shown in Fig. 1b, 1c, pre-existing Pt-NPs greatly improve growing uniformity of the Pt nanowires by comparing with pure carbon case in Fig. 1a. This is due to that the pre-existing Pt nanoparticles not only provide low energy interfaces for Pt nucleation, trigger the nucleation and anisotropic growth of the Pt-NPs liking Au<sup>35</sup> or Pd seeds<sup>36</sup>, but also may act as catalyst for the Pt reduction reaction. It was reported that Pd nanoparticles on the beads (a substrate) could acted as catalytic sites for the anisotropic Pt growth, and once the growth was initiated, the Pt nanowires continually grew in the  $\langle 111 \rangle$  direction until the supply of Pt<sup>0</sup> atoms was depleted.<sup>37</sup> It can be found obviously in the high-resolution TEM insets of Fig. 1(a)~(c) that with increasing the Pt nanoparticles in the carbon matrix the Pt-NWs are shorter and evenly tends unordered. This proves the existent Pt-NPs functioned as growing sites for Pt nanowires.

Fig.1

To illustrate the effect of Pt-NPs on Pt-NW crystallinity, the XRD patterns of the Pt nanowire electrodes with the Pt-NP loadings of 0, 0.005 and  $0.010\text{mg}_{\text{Pt-NP}}\text{cm}^{-2}$  were measured and shown in Fig. 2. All XRD patterns of the samples are similar with bulk platinum and Pt characteristic peaks appear at  $2\theta$  of  $39.8^\circ$ ,  $46.3^\circ$ ,  $67.5^\circ$  and  $81.6^\circ$ , respectively corresponding to the (111), (200), (220), and (311) facets. The samples at the Pt-NP loadings of 0 and  $0.005\text{mg}_{\text{Pt}}\text{cm}^{-2}$  have sharp and intense peaks of the (111) facet, which means perfect crystallinity and dominant (111) facets. However, more seeds liking the Pt-NP loading of  $0.010\text{mg cm}^{-2}$  introduce more growing sites, and lead less crystallinity or amorphous structure, which is again in well agreement with the above TEM analysis.

Fig. 2

The carbon matrix thickness, which linearly increases with carbon loadings, affected Pt nanowire distribution as Pt precursor diffuses into through the matrix micro-pores from the bulk solution. To examine Pt nanowire dispersions of various carbon loadings of 0.10, 0.20 and 0.30  $\text{mg}_C \text{cm}^{-2}$ , the TEM images near the GDLs region were photographed, where the least Pt nanowires were formed as the lowest concentrations of Pt precursor. The diffusion effect of formic acid can be ignored as it is extremely excessive ( $>100$  stoichiometric ratio). As shown in Fig. 1(d) ~ (f), the sample with the highest carbon loading of 0.30  $\text{mg}_C \text{cm}^{-2}$  has the thickest catalyst layer and the least Pt-NWs in the region near the GDE. By comparing with blank carbon as shown in Fig. 1(a), the Pt-NPs improve uniformity of Pt nanowires growing along the Pt-NW matrix thickness as depth as  $>10\mu\text{m}$  (i.e. carbon loading of 0.30  $\text{mg}_C \text{cm}^{-2}$ ).

#### Single cell performances improved by Pt nanoparticles

The polarization curves of various single cells with the commercial GDE and home-made Pt-NW cathodes are shown in Fig. 3. The Pt-NP loading of the Pt-NW cathodes is varied from 0 to 0.010  $\text{mg}_{\text{Pt-NP}} \text{cm}^{-2}$  as shown in Fig. 3(a). The optimal Pt-NP loading is obtained at 0.005  $\text{mg}_{\text{Pt-NP}} \text{cm}^{-2}$  with the current density 1.29  $\text{A cm}^{-2}$  at 0.60 V. Comparing the cell performances of the commercial GDE and the optimal Pt-NW cathode, there is a crossing point at cell voltage of 0.48 V. When the voltage is below 0.48V, the optimal Pt-NW cathode has better performance, i.e. lower concentration polarization loss, for example, its current density at 0.30 V is 7% higher than that of the commercial GDE. The lower concentration polarization is accredited to the Pt-NWs openly exposed to oxidant, not liking that in the conventional electrodes part of Pt nanoparticles lost in the dead pores or very narrow pores and cannot be accessed. On the other hand, at a higher voltage over 0.48 V, the performance of the Pt-NW cathode is slightly lower, for example, its current density at 0.60 V is about 5% lower than that of the commercial GDE. This poorer performance of the Pt-NW cathode at high voltage range may be due to its lower Pt catalyst loading,<sup>38</sup> where the Pt loading ratio of the optimal Pt-NW cathode and the commercial cathode is 0.205  $\text{mg}_{\text{Pt}} \text{cm}^{-2}$  vs 0.40  $\text{mg}_{\text{Pt}} \text{cm}^{-2}$ .

Fig. 3

EIS experiments were carried out to further evaluate the cathodes performances. Fig. 4(a) and 4(b) shows the EIS results of various Pt-NP loadings at the cell voltages of 0.80 and 0.40 V, respectively. At 0.80 V, due to the lower current density, the cathode impedances are dominated by the charge transfer resistances which are represented by the arc diameters in the Nyquist plots. The commercial GDE exhibits the smallest arc diameter, indicating the smallest charge transfer resistance and the best ORR kinetics, which corresponding to the highest current density in the high voltage range. Meanwhile, among the Pt-NW cathodes, the Pt-NW cathode with 0.005  $\text{mg}_{\text{Pt-NP}} \text{cm}^{-2}$  has the smallest charge transfer resistance, even if its Pt loading is less than that of the cathode with 0.010  $\text{mg}_{\text{Pt-NP}} \text{cm}^{-2}$ . This is due to more active (111) facets of the former supported by Fig. 2. At 0.40 V, there are two semi-circles for all samples. The high frequency arc (left) is attributed to the charge transfer impedance and double layer capacitance, and the low frequency arc (right) is related with the mass transfer resistance.<sup>39</sup> The cathode with 0.005  $\text{mg}_{\text{Pt-NP}} \text{cm}^{-2}$  has the smallest diameter of low frequency arc compared with all the other

samples, even including the commercial GDE, confirming the smallest mass transfer resistance and best performance.

Fig. 4

The Pt-NP effect on the CV curves and ECSA values of the Pt-NW cathodes are illustrated in Fig. 5(a). The ECSA value increases with the Pt-NP loading, and the maximum value of  $41.94 \text{ m}^2 \text{ g}_{\text{Pt}}^{-1}$  is achieved at a Pt-NP loading of  $0.010 \text{ mg}_{\text{Pt-NP}} \text{ cm}^{-2}$ , and the minimum value of  $36.72 \text{ m}^2 \text{ g}_{\text{Pt}}^{-1}$  at no Pt-NPs added. This trend meets with the results from TEM images in Fig. 1(a) ~ (c) and XRD patterns in Fig. 2. The increase of the ECSA value with Pt-NP loading can be attributed to the more growing/depositing sites, and therefore the Pt-NW length and the catalyst aggregation is decreased. However, at a high Pt-NP loading, such as  $0.010 \text{ mg}_{\text{Pt-NP}} \text{ cm}^{-2}$ , the excessive growing sites lead to lower Pt-NW crystallinity, presenting an indistinct crystallographic alignment as shown in the inset of Fig.1c, and finally resulting in a large charge transfer resistance and a low ORR activity.

Fig. 5

#### Effects of matrix carbon loadings on single cell performance

The carbon loading in the matrix determines the cathode thickness, and there is a linear relationship between them.<sup>40</sup> There is a balance between the mass transfer resistance and Pt-NW aggregation. Performance curves of the Pt-NW cathodes with different carbon loadings are shown in Fig. 3(b). The performance curves of the Pt-NW cathode with  $0.10 \text{ mg}_C \text{ cm}^{-2}$  and  $0.20 \text{ mg}_C \text{ cm}^{-2}$  are quite similar, for example, their current densities at  $0.60 \text{ V}$  are about  $1.35 \text{ A cm}^{-2}$ . Among the Pt-NW cathodes, the  $0.10 \text{ mg}_C \text{ cm}^{-2}$  one is the highest power density at the cell voltage  $> 0.53 \text{ V}$ , while the  $0.20 \text{ mg}_C \text{ cm}^{-2}$  one the best at the cell voltage  $< 0.53 \text{ V}$ . The Pt-NW cathode with  $0.30 \text{ mg}_C \text{ cm}^{-2}$  exhibits the poorest performance, which means that the thick cathode causes deleterious mass transfer polarization.

The EIS results of the Pt-NW cathodes with different carbon loadings are illustrated in Fig. 4(c) and 4(d). It can be seen that, the cathode with  $0.10 \text{ mg}_C \text{ cm}^{-2}$  has the smallest impedance at  $0.80 \text{ V}$  while one with  $0.3 \text{ mg}_C \text{ cm}^{-2}$  has the largest impedance at  $0.40 \text{ V}$ , suggesting their smallest charge transfer resistance and the largest mass transfer resistance, respectively. The cathode with  $0.20 \text{ mg}_C \text{ cm}^{-2}$  exhibits the smallest mass transfer resistance at  $0.40 \text{ V}$ . Hence, the  $0.20 \text{ mg}_C \text{ cm}^{-2}$  one has an optimal performance at low voltage range.

To further investigate the effect of carbon contents, the cycle voltammograms were recorded to evaluate the electrode ECSAs, and the results are presented in Fig. 5(b). The maximum ECSA value is  $58.06 \text{ m}^2 \text{ g}_{\text{Pt}}^{-1}$  obtained at  $0.10 \text{ mg}_C \text{ cm}^{-2}$ , and drops to  $27.85 \text{ m}^2 \text{ g}_{\text{Pt}}^{-1}$  when the carbon loading is  $0.30 \text{ mg}_C \text{ cm}^{-2}$ . This can reason that the ionomer sprayed cannot reach on the deep Pt-NWs which could not contribute to electrochemistry. The value of  $58.06 \text{ m}^2 \text{ g}_{\text{Pt}}^{-1}$  is even higher than that of  $47.0 \text{ m}^2 \text{ g}_{\text{Pt}}^{-1}$  of the conventional Pt/C electrode reported in our previous work.<sup>30</sup> However, except of ECSA, the cathode reaction also depends on conductivity and oxygen supplying. Therefore, the optimal carbon loading is  $0.20 \text{ mg}_C \text{ cm}^{-2}$ .

#### Pt efficiency comparing



Catalyst activity measurements of MEAs are generally evaluated using H<sub>2</sub>/O<sub>2</sub> reactants in order to minimize mass transport resistances.<sup>41</sup> To comparing Pt efficiency under real H<sub>2</sub>/air operating conditions, here the current density data at 0.9 V were taken and the specific current densities (SCDs) on Pt mass basis were calculated according to the data from Fig. 3(a). The SCDs of the home-made Pt-NW cathodes with Pt seeds loadings of 0, 0.005, and 0.010 mg<sub>Pt-NP</sub> cm<sup>-2</sup> and the commercial GDE are summarized in Table 1. The Pt-NW cathode with 0.005 mg<sub>Pt-NP</sub> cm<sup>-2</sup> has the highest SCD value of 89.56 A g<sub>Pt</sub><sup>-1</sup>, which is 47 % higher than 60.95 A g<sub>Pt</sub><sup>-1</sup> of the 0.010 mg<sub>Pt-NP</sub> cm<sup>-2</sup> one and 110% higher than 42.58 A g<sub>Pt</sub><sup>-1</sup> of the commercial GDE. The 0.005 mg<sub>Pt-NP</sub> cm<sup>-2</sup> one has the optimal catalyst utilization, although its ECSA value is a little smaller than that of the 0.010 mg<sub>Pt-NP</sub> cm<sup>-2</sup> sample. The SCD value of the commercial GDE is the smallest, and is less half of the 0.005 mg Pt-NP cm<sup>-2</sup> sample. The high Pt efficiency of the Pt-NW cathodes is according to: i) Pt-NWs grow directly on the pore wall almost with no hiding; ii) P-NP seeds induce uniform growing of Pt-NWs; and iii) dominant (111) facets with high catalytic activity for oxygen reduction reaction (ORR).

Table 1

#### **Mechanism of Pt nanowires growing on Pt nanoparticle seeds**

There are many mechanisms of nucleation and growth in solutions such as LaMer nucleation, Finke-Watzky two step mechanism, Ostwald ripening, digestive ripening, coalescence and orientated attachment, and intra-particle growth.<sup>28</sup> However, these mechanisms are in conflicts or inverse with some others, for example, the nucleation and growth could occur simultaneously by Finke-Watzky mechanism or separately by LaMer mechanism. Cheong et al<sup>42</sup> investigated the precursor concentrations effects by in situ and ex situ methods and found the low concentration growth occurs at a relatively slow rate and yields faceted morphologies, are characteristic of a thermodynamically controlled regime. It is thought that incomplete reduction of AuCl precursor allows only a part of it to transform to Au, which can seed nanowire growth.<sup>43</sup> Meng et al<sup>16</sup> demonstrated that both formate as the intermediate species and HCOOH in the reacting solution (PH=1.5~3.5) are significantly important, while formate reduces the Pt salt and HCOOH block all Pt surfaces except Pt (111) facets.

The catalytic phenomena of Pt-NP seeds was observed obviously in present experimental. When Pt-NPs (supported on carbon) added in the matrix, the color of the solution containing Pt precursor fades from light yellow to colorless in less than 12hrs, comparing that more than 24hrs without Pt-NPs. The proposed schematic of Pt nanowires growth mechanism in the carbon matrix is illustrated in Fig. 6. It is assumed that the platinum precursors and formic acid diffuse into the the matrix consisting of carbon powders and Pt-NPs bonded by ionomer. Then the Pt seeds facilitate platinum precursor reduction and provide depositing sites for the newly formed Pt atoms which are nearly layer-by-layer monomer addition onto the crystallite faces to yield stable morphology. Except of reducing function, overwhelming formic acid also serves for capping agent, therefore platinum atoms add onto the (111) facet and the sole nanowire morphology were produced. Concentration difference of platinum precursor, driving from the bulk into the matrix through the micro pores, leads to a gradient Pt-NW profile. Nanocrystal growth

in the low concentration reaction, here 1mM chloroplatinic acid hexahydrate adopted, occurs under thermodynamic control.<sup>42</sup> Here weak reducing agent, low concentrations of the reactants and low temperature ensure a slow reaction rate. Formic acid as capping agent plays an important role and promotes an anisotropy growth along (111) facets.<sup>16</sup> On the other hand, catalytic and seed functions of Pt-NPs induce Pt atoms deposited preferentially on the Pt-NPs, not carbon particles, and result in relatively progressive gradient or better uniformity along the matrix thickness. It was evidenced by the results of the TEM images and XRD patterns as shown in Fig. 1(a)~(c) and Fig. 2, where the more Pt-NP seeds, the shorter nanowires at the same Pt depositing amount.

Fig. 6

## Conclusions

In summary, a novel Pt-NW cathode with low Pt loading was developed by introducing Pt nanoparticles (Pt-NPs) into a carbon matrix and in-situ growing Pt nanowires. The pre-existing Pt nanoparticles provide low energy interfaces for Pt nucleation and thus induce the Pt nanowire growth, therefore avoid the Pt nanowire aggregation. However, excessive Pt nanoparticles decrease length and crystallinity of the Pt nanowires, even if resulting in an amorphous structure. The carbon loading in the matrix dominates the matrix thickness and Pt profile. The optimal Pt-NW cathode is with Pt-NP loading of  $0.005 \text{ mg}_{\text{Pt-NP}} \text{ cm}^{-2}$  and carbon loading of  $0.02 \text{ mg}_{\text{C}} \text{ cm}^{-2}$ , respectively. The optimal cathode with total cathode Pt loading of  $0.205 \text{ mg cm}^{-2}$  has the highest specific current density of  $89.56 \text{ A g}_{\text{Pt}}^{-1}$  at 0.9V under air/H<sub>2</sub> feeding, which is about 110% higher than that of the commercial GDE with Pt loading of  $0.40 \text{ mg cm}^{-2}$ . When the cell voltage is below 0.48V, the optimal Pt-NW cathode has better performance than the commercial GDE. Good performance of the Pt-NW cathodes was attributed to i) uniform Pt-NW growth induced by Pt-NPs; ii) high Pt utilization as Pt-NWs growing directly on the pore wall and hence fully exposed to oxidant iii) dominant (111) facets of the Pt-NWs with high ORR catalytic activity. A Pt-NW growth mechanism was proposed that Pt precursor diffuses into the matrix of pre-existing Pt-NPs by concentration driving, and Pt-NPs as seeds induce Pt-NW growth kinetics and provide priority sites for platinum depositing. This work provides a new strategy for tailoring Pt-NW nanostructures and designing the electrode architectures, and can be extended to the other electrocatalysts of alloys or alloying nanowires.

## Acknowledgements

We gratefully acknowledge the financial supports from the *European Union's Horizon 2020 research and innovation programme H2020-MSCA-IF-2014* under grant agreement No 658217, *the National Natural Science Foundation of China* under grant agreement No 21576164, *and the International Science & Technology Cooperation Program of the Ministry of Science & Technology* (grant No. 2015DFG62250).

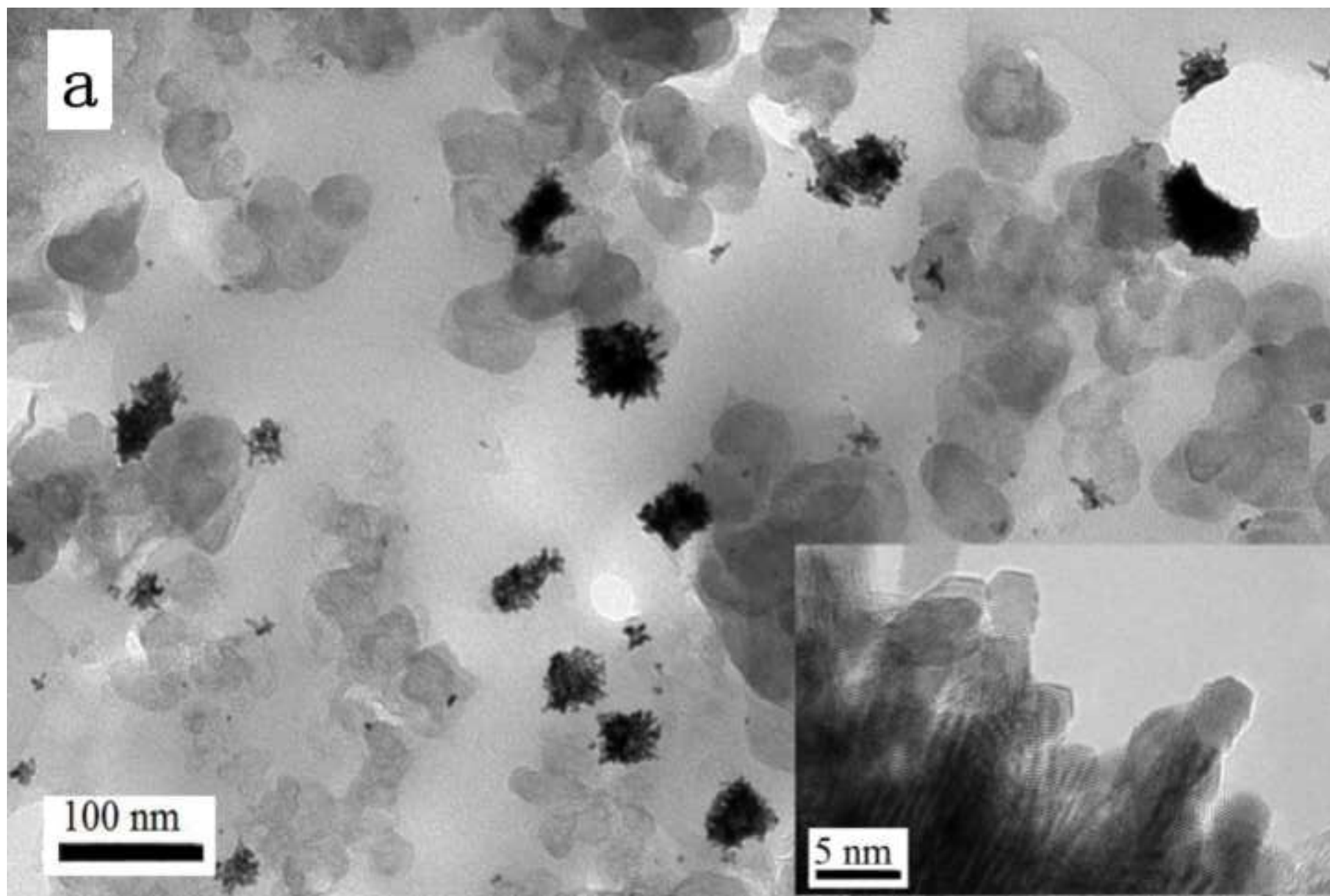
## references

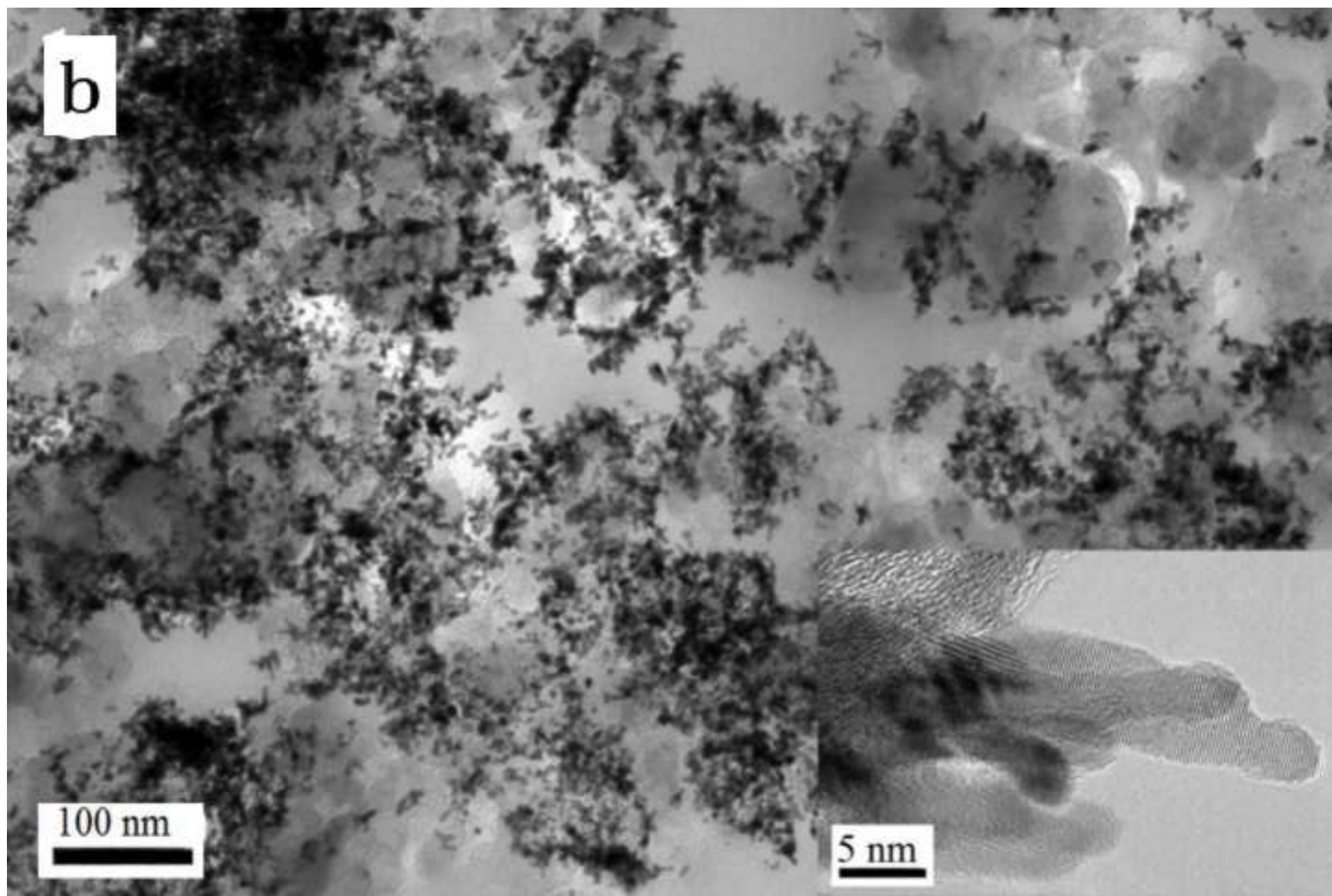
- 1 Ifan Erfyl Lester Stephens, Jan Rossmeisl and Ib Chorkendorff, *Science*, 2016, 354 (6318), 1378.
- 2 Xiaoqing Huang, Zipeng Zhao, Liang Cao, Yu Chen, Enbo Zhu, Zhaoyang Lin, Mufan Li, Aiming Yan, Alex Zettl, Y. Morris Wang, Xiangfeng Duan, Tim Mueller and Yu Huang, *Science*, 2015, 348(6240), 1230.
- 3 Sheng Sui, Xiaoying Wang, Xintong Zhou, Yuehong Su, Saffa B Riffat and Chang-jun Liu, *J. Mater. Chem. A*, 2017, 5, 1808.
- 4 Batyr Garlyyev, Marcus D Pohl, Viktor Čolić, Yunchang Liang, Faheem K Butt, Alexander Holleitner, and Aliaksandr S Bandarenka, *Electrochem. Commun.*, 2018, 88, 10.
- 5 NamgeeJung, Dong YoungChung, JaeyuneRyu, Sung JongYoo and Yung-EunSung, *Nano Today*, 2014, 9, 433.
- 6 Laetitia Dubau, Miguel Lopez-Haro, Julien Durst, Laure Guétaz, Pascale Bayle-Guillemaud, Marian Chatenetab and Frédéric Maillard, *J. Mater. Chem. A*, 2014, 2, 18497
- 7 Yijin Kang, Peidong Yang, Nenad M. Markovic and Vojislav R. Stamenkovic, *Nano Today*, 2016, 11, 587.
- 8 María Escudero-Escribano, Paolo Malacrida, Martin H. Hansen, Ulrik G. Vej-Hansen, Amado Velázquez-Palenzuela, Vladimir Tripkovic, Jakob Schiøtz, Jan Rossmeisl, Ifan E. L. Stephens and Ib Chorkendorff, *Science*, 2016, 352(6281), 73.
- 9 Tim Van Cleve, Saman Moniri, Gabrielle Belok, Karren L. More and Suljo Linic, *ACS Catal.*, 2017, 7, 17.
- 10 Arup Mahata, Kuber Singh Rawat, Indrani Choudhuri and Biswarup Pathak, *J. Mater. Chem. A*, 2016, 4, 12756.
- 11 Muhammad Aurang Zeb Gul Sial, Muhammad Aizaz Ud Din and Xun Wang, *Chem. Soc. Rev.*, 2018, DOI: 10.1039/c8cs00113h
- 12 Wei Wang, Fan Lv, Bo Lei, Sheng Wan, Mingchuan Luo and Shaojun Guo, *Adv. Mater.*, 2016, 28, 10117.
- 13 BY Xia, HB Wu, N Li, Y Yan, XW Lou and X Wang, *Angew. Chem. Int. Ed.*, 2015, 54(12), 3797.
- 14 Yaxiang Lu, Shangfeng Du and Robert Steinberger-Wilckens, *Appl. Catal. B: Environ.*, 2016, 199, 292.
- 15 Yameng Wang, Liangliang Zou, Qinghong Huang, Zhiqing Zou and Hui Yang, *Int. J. Hydrogen Energy*, 2017, 42(43), 26695.
- 16 Hui Meng , Yunfeng Zhan , Dongrong Zeng , Xiaoxue Zhang , Guoqing Zhang and Frédéric Jaouen, *small*, 2015, 11(27), 3377.
- 17 Hai-Wei Liang, Xiang Cao, Fei Zhou, Chun-Hua Cui, Wen-Jun Zhang and Shu-Hong Yu, *Adv. Mater.*, 2011, 23, 1467.
- 18 HJ Kim, YS Kim, MH Seo, SM Choi, J Cho, GW Huber and WB Kim, *Electrochem. Commun.*, 2010,12(1), 32.
- 19 Robert Wainright and Ramaraja P. Ramasamy, *J. Electrochem. Soc.*, 2016, 163 (6), F533.
- 20 Fangfang Chang, Gang Yu, Shiyao Shan, Zakiya Skeete, Jinfang Wu, Jin Luo, Yang Ren, Valeri Petkov and Chuan-Jian Zhong, *J. Mater. Chem. A*, 2017, 5, 12557.
- 21 Mingchuan Luo, Yingjun Sun, Xu Zhang, Yingnan Qin, Mingqiang Li, Yingjie Li, Chunji Li, Yong Yang, Lei Wang, Peng Gao, Gang Lu and Shaojun Guo, *Adv. Mater.*, 2018, 30, 1705515
- 22 T. Nguyen, K. Thanh, N. Maclean and S. Mahiddine, *Chem. Rev.*, 2014, 114, 7610
- 23 Fang Gao, Nianjun Yang, Waldemar Smirnov, Harald Obloh and Christoph E. Nebel, *Electrochim. Acta*, 2013, 90, 445.

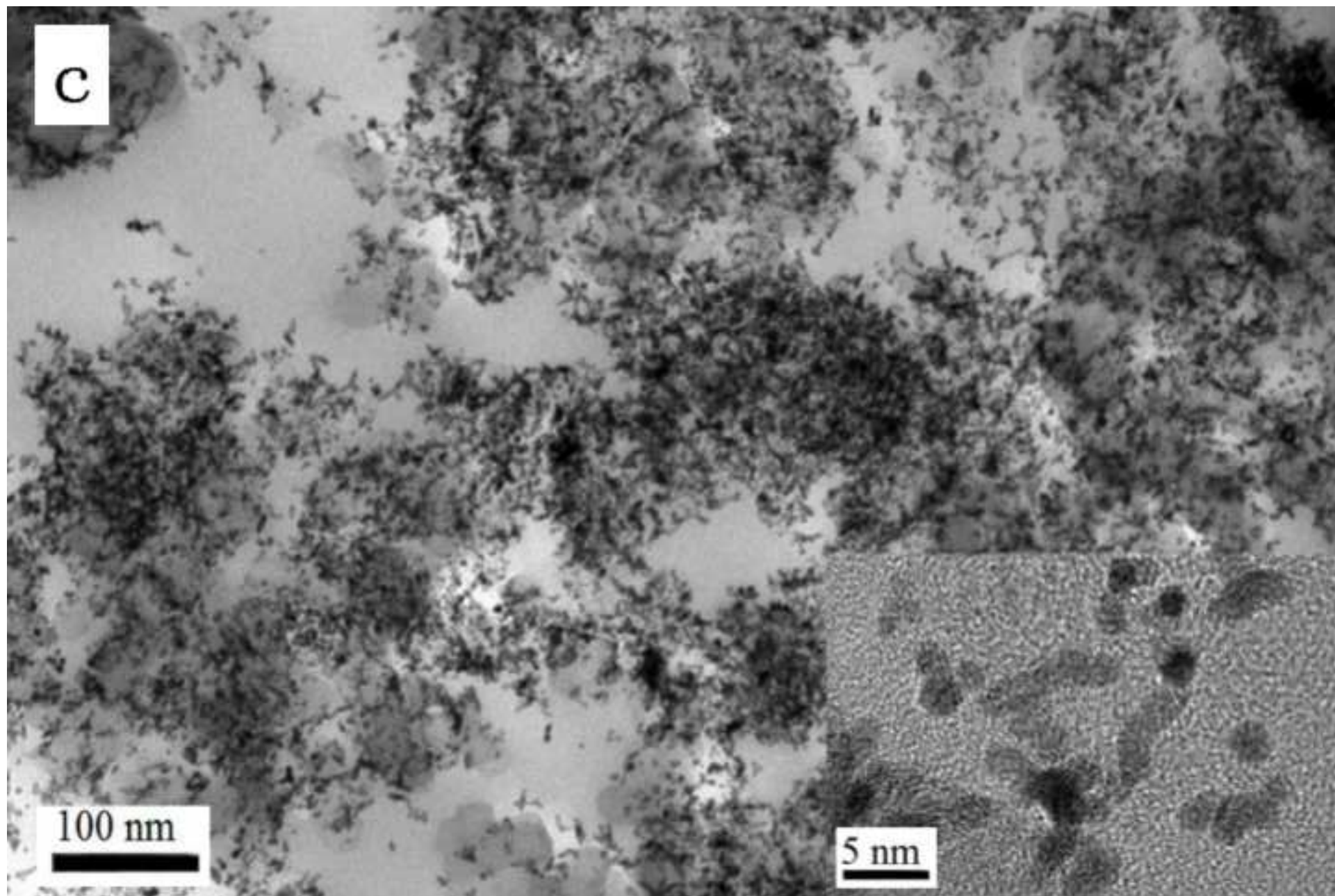
- 24 Simona E. Hunyadi Murph, Catherine J. Murphy, Austin Leach and Kenneth Gall, *Cryst. Growth Des.*, 2015, 15, 1968.
- 25 Younan Xia, Yujie Xiong, Byungkwon Lim and Sara E. Skrabalak, *Angew. Chem. Int. Ed.*, 2008, 47, 2.
- 26 S. Litster, W. K. Epting, E. A. Wargo, S. R. Kalidindi and E. C. Kumbur, *Fuel Cells*, 2013, 13(5), 935.
- 27 Gokce S. Avcioglu, Berker Ficilar and Inci Eroglu, *Int. J. Hydrogen Energy*, 2018, 43(23), 10779.
- 28 Zhangxun Xia, Suli Wang, Luhua Jiang, Hai Sun, Fulai Qi, Jutao Jin, Gongquan Sun, *J. Mater. Chem. A*, 2015, 3, 1641.
- 29 Giorgio Ercolano, Filippo Farina, Sara Cavaliere, Deborah J. Jones and Jacques Rozière, *J. Mater. Chem. A*, 2017, 5, 3974
- 30 Xianyong Yao, Kaihua Su, Sheng Sui, Liwei Mao, An He, Junliang Zhang and Shangfeng Du, *Int. J. Hydrogen Energy*, 2013, 38(28), 12374.
- 31 Zhaoxu Wei, An He, Kaihua Su, Sheng Sui, *J. Energy Chem.*, 2015, 24(2), 213.
- 32 K Su, X Yao, S Sui, Z Wei, J Zhang and S Du, *Fuel Cells*, 2015, 15(3), 449.
- 33 Xuhai Wang, Francis W. Richey, Kevin H. Wujcik and Yossef A. Elabd, *J. Power Sources*, 2014, 264, 42.
- 34 Zheng Fang, Yuliang Zhang, Feifei Du and Xinhua Zhong, *Nano. Res.*, 2008, 1, 249.
- 35 Gilles Berhault, Marta Bausach, Laure Bisson, Loïc Becerra, Cécile Thomazeau and Denis Uzio, *J. Phys. Chem. C*, 2007, 111, 5915.
- 36 Eric P. Lee, Jingyi Chen, Yadong Yin, Charles T. Campbell and Younan Xia, *Adv. Mater.*, 2006, 18, 3271.
- 37 S Du and BG Pollet, *Int. J. Hydrogen Energy*, 2012, 37, 17892.
- 38 Mariana Ciureanu and Raymond Roberge, *J. Phys. Chem. B*, 2001, 105, 3531.
- 39 Kaihua Su, Sheng Sui, Xianyong Yao, Zhaoxu Wei, Junliang Zhang and Shangfeng Du, *Int. J. Hydrogen Energy*, 2014, 39, 3397.
- 40 Hubert A. Gasteiger, Shyam S. Kocha, Bhaskar Sompalli and Frederick T. Wagner, *Appl. Catal. B: Environ.*, 2005, 56, 9.
- 41 Hubert A. Gasteiger, Shyam S. Kocha, Bhaskar Sompalli and Frederick T. Wagner, *Appl. Catal. B: Environ.*, 2005, 56, 9.
- 42 Soshan Cheong, John Watt, Bridget Ingham, Michael F. Toney and Richard D. Tilley, *J. Am. Chem. Soc.*, 2009, 131, 14590.
- 43 Paromita Kundu, Aditi Halder, B. Viswanath, Dipan Kundu, Ganpati Ramanath and N. Ravishankar, *J. Am. Chem. Soc.*, 2010, 132, 20.

**Table 1**

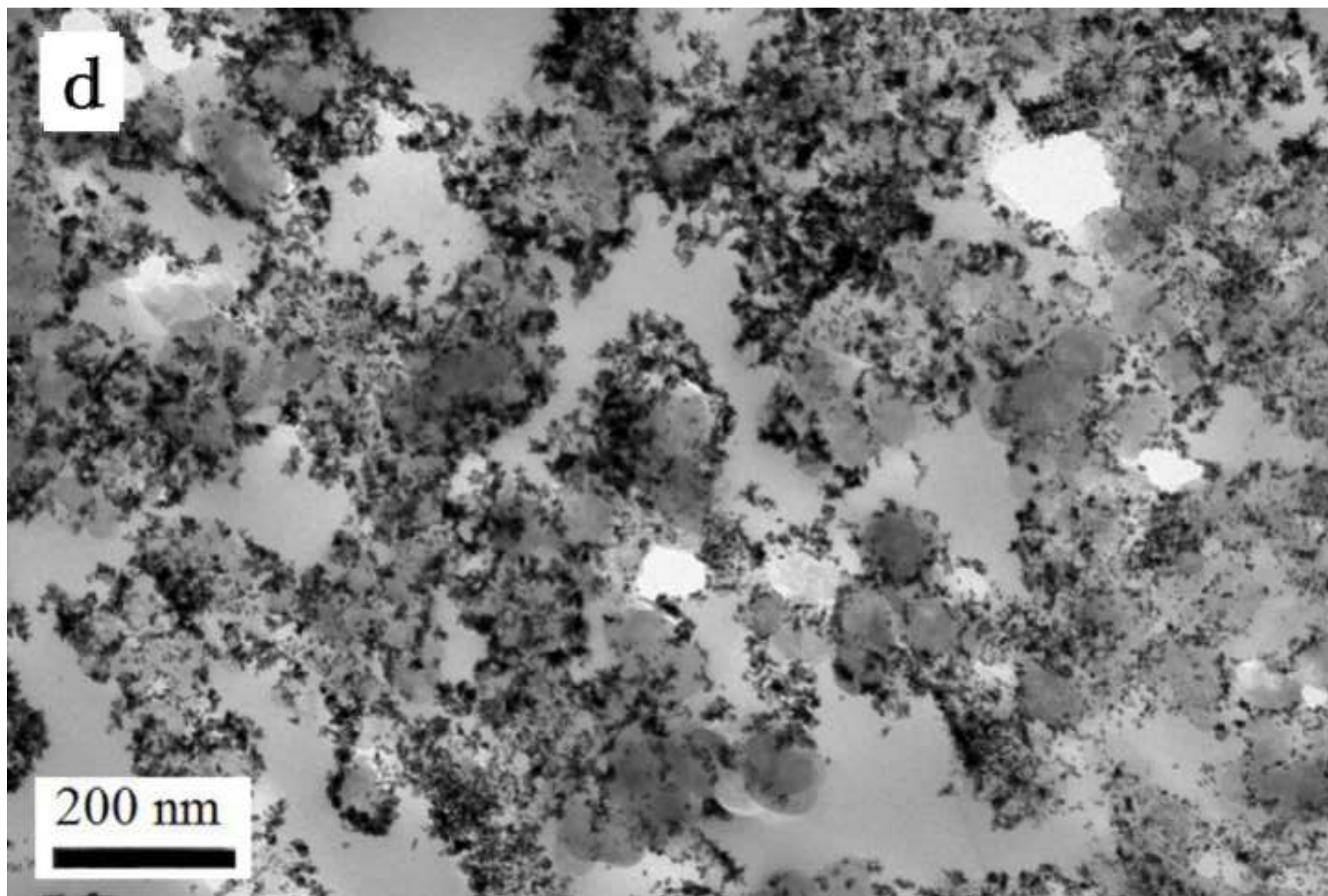
Cathode Pt loading [m]/mg <sub>Pt</sub> cm <sup>-2</sup>	Current density [j]/mA cm <sup>-2</sup>	Specific current density(SCD) with Pt mass [j <sub>m</sub> ]/A g <sub>Pt</sub> <sup>-1</sup>	Specific current density(SCD) with Pt ECSA [j <sub>s</sub> ]/A m <sub>Pt</sub> <sup>-2</sup>
Pt-NWs (0.2)	15.34	76.70	2.09
Pt-NWs (0.2)+Pt-NP (0.005)	18.36	89.56	2.14
Pt-NWs (0.2)+Pt-NP (0.010)	12.80	60.95	1.66
Commercial GDE (0.4)	17.03	42.58	0.91

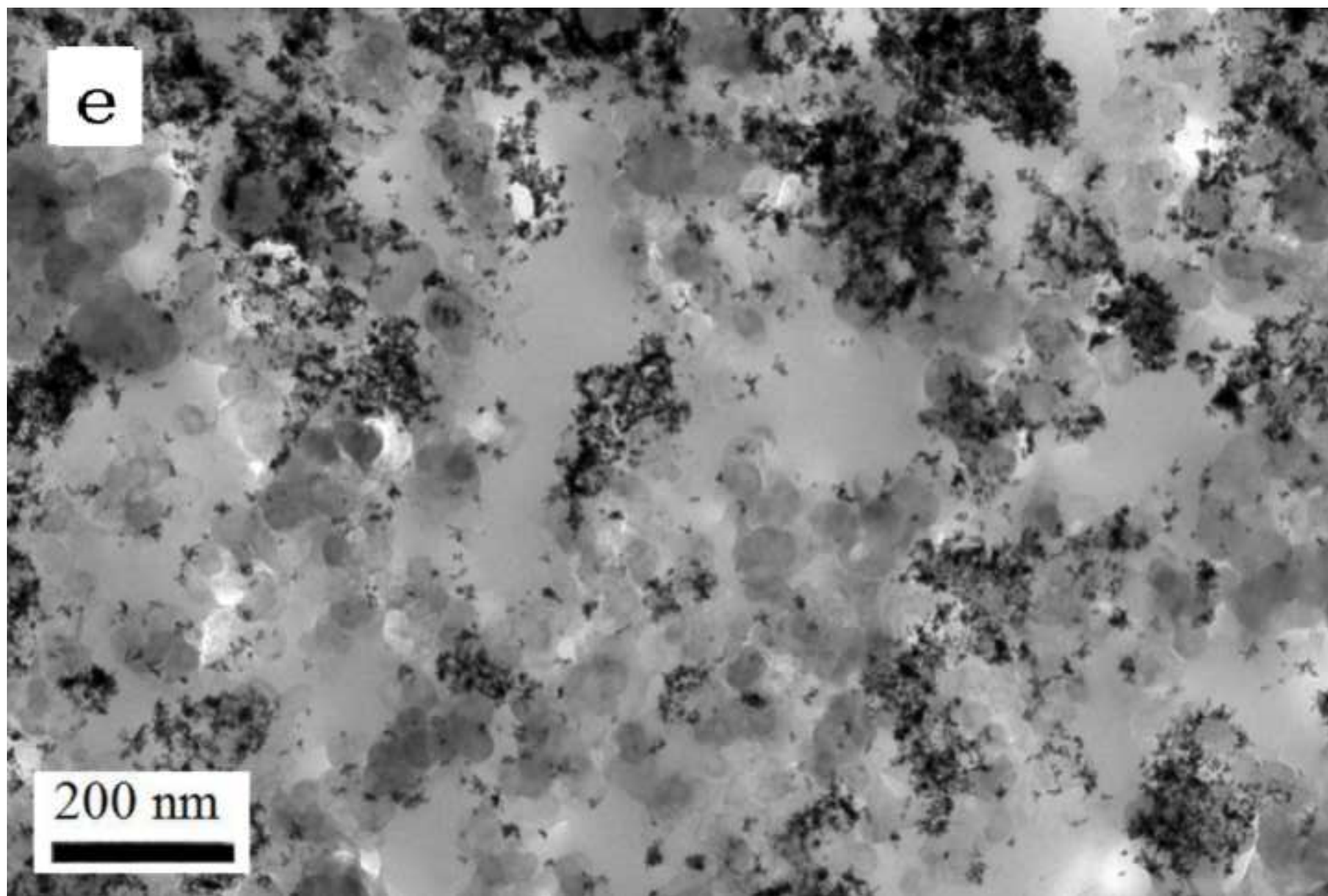












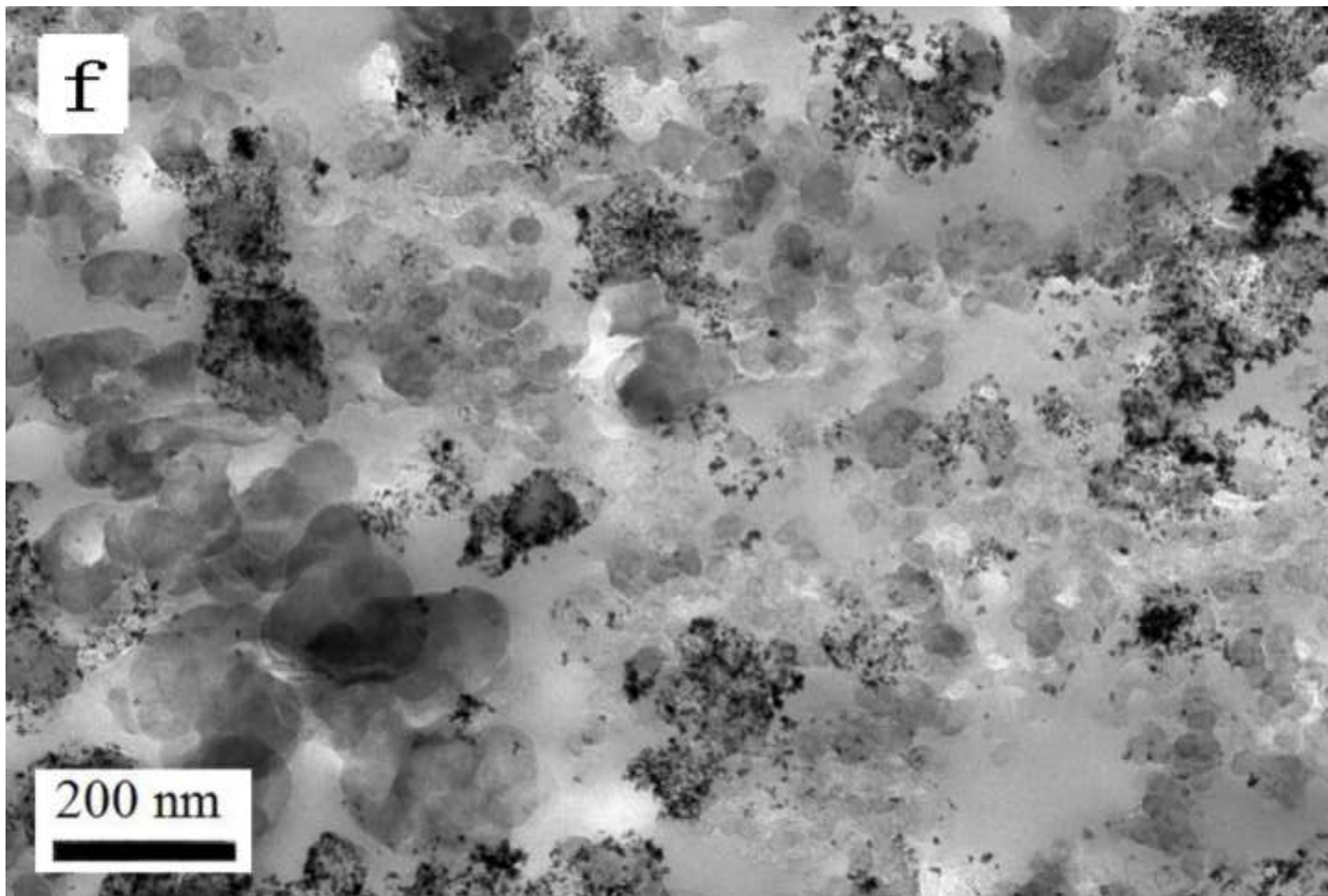
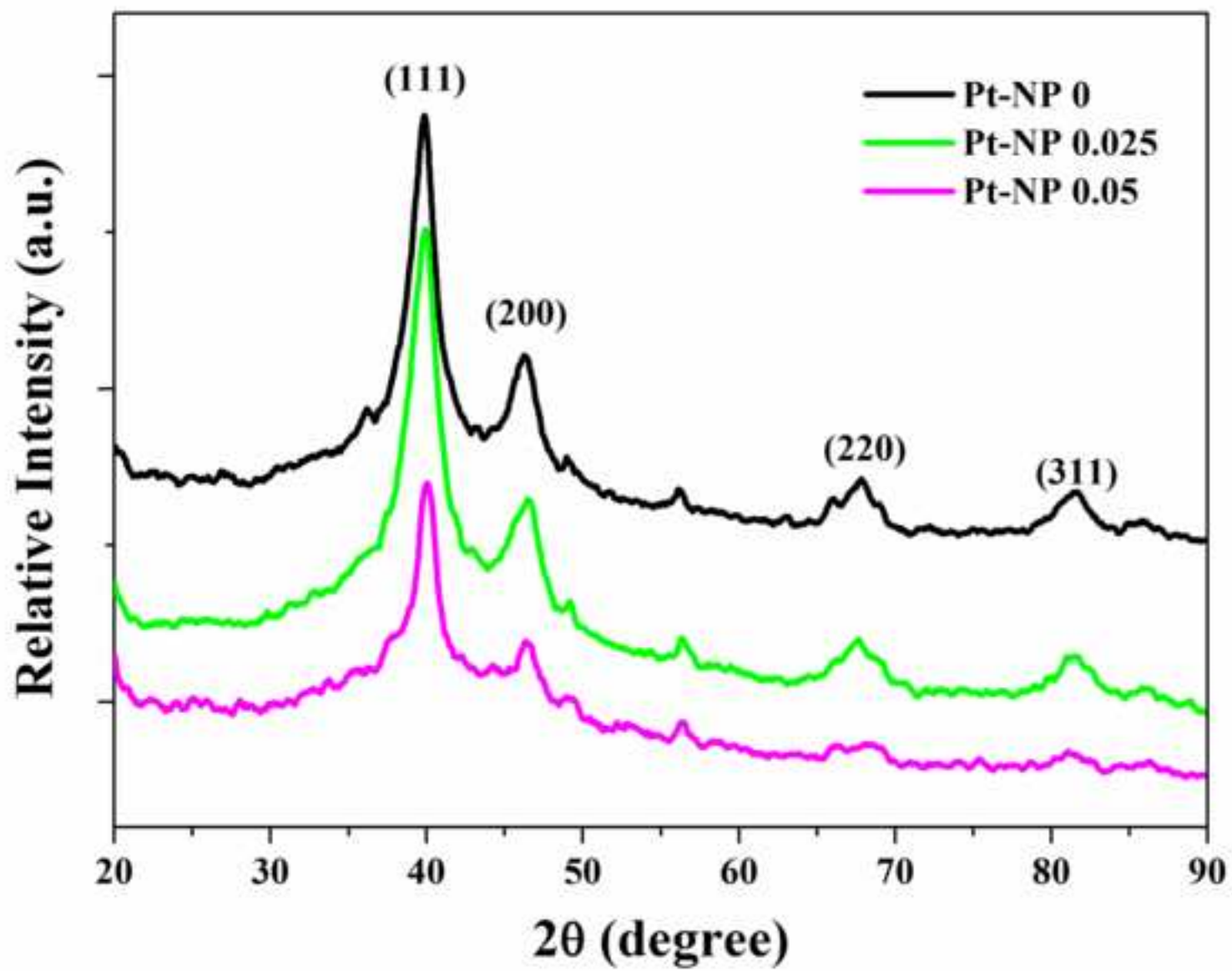
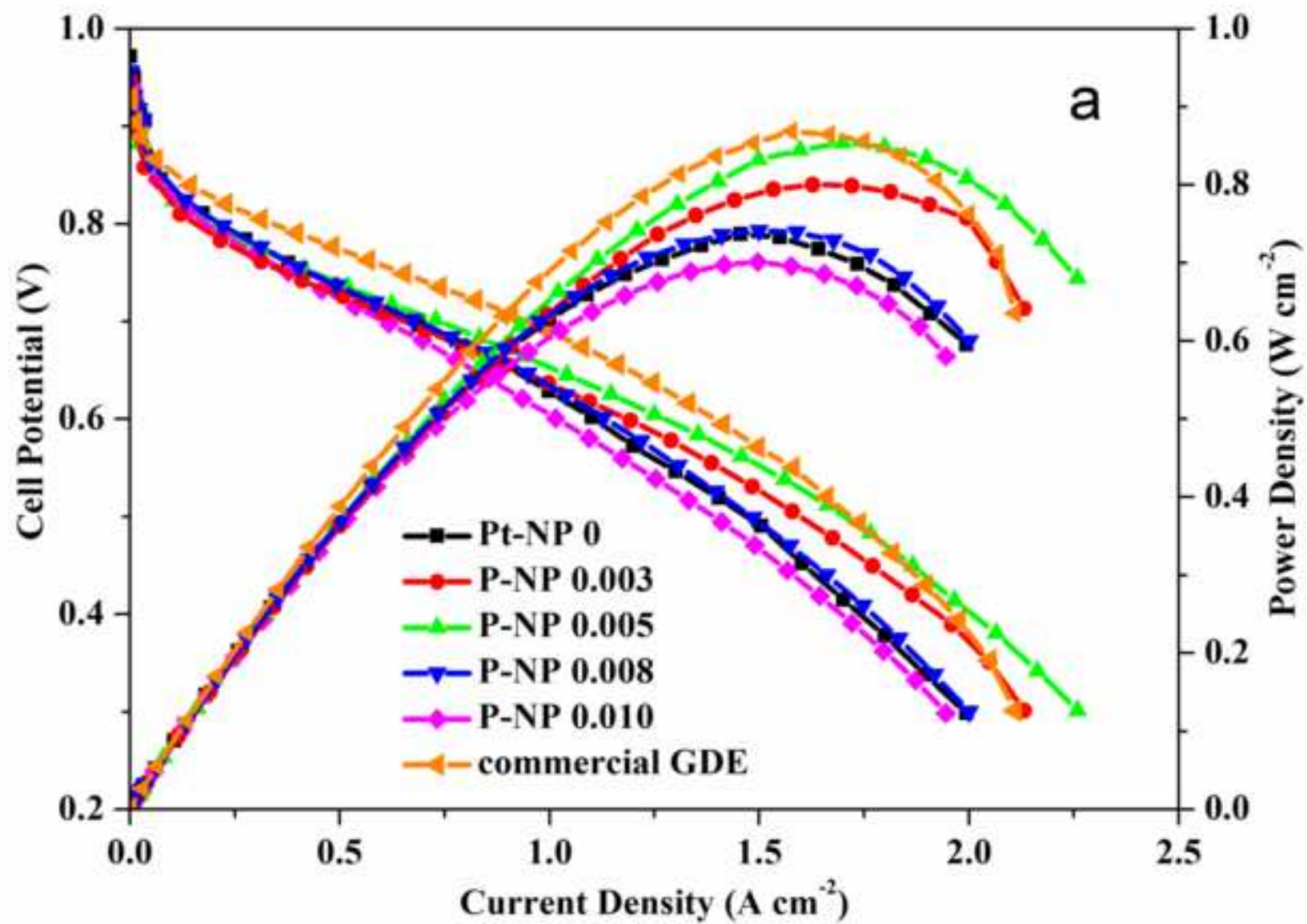
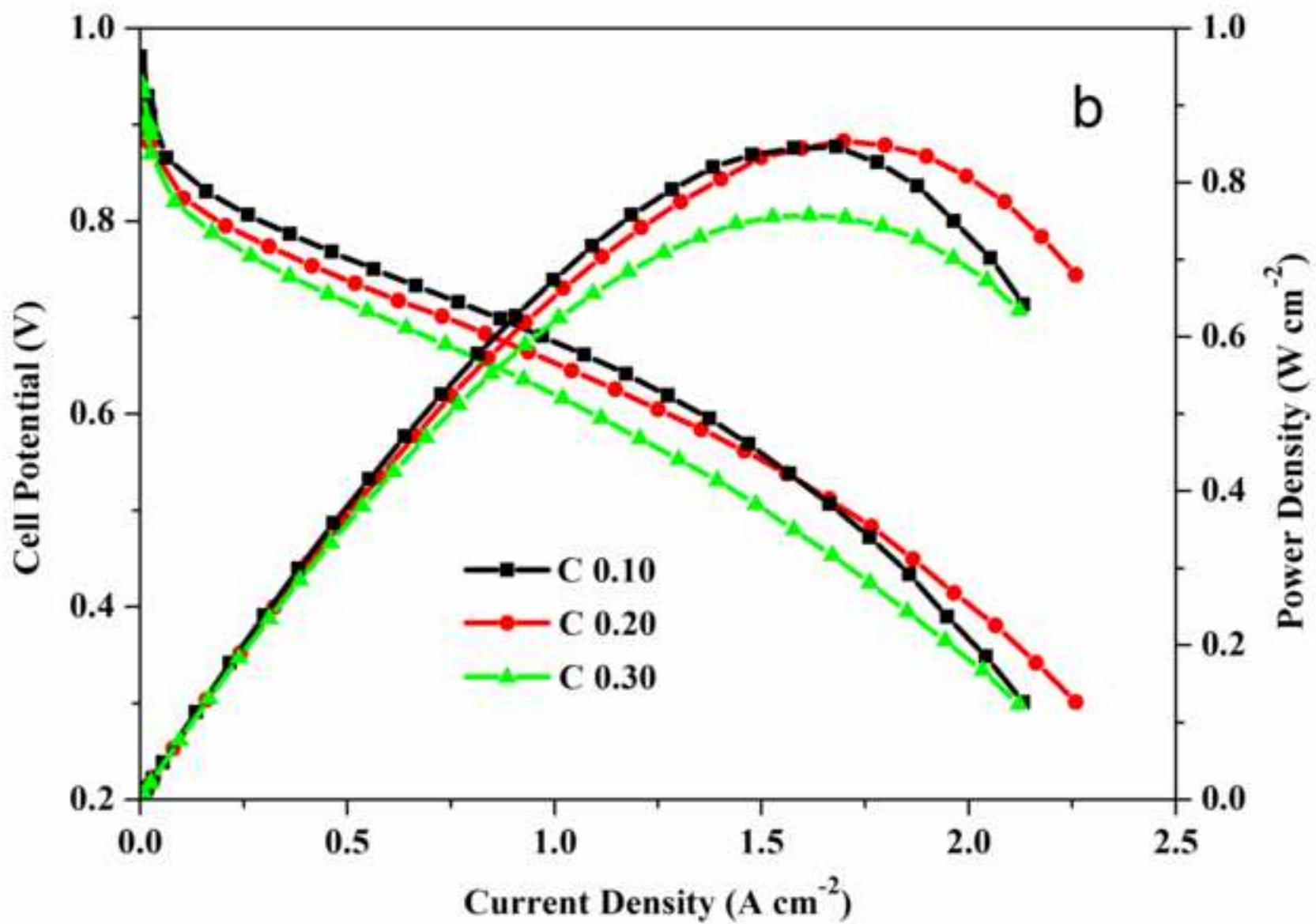
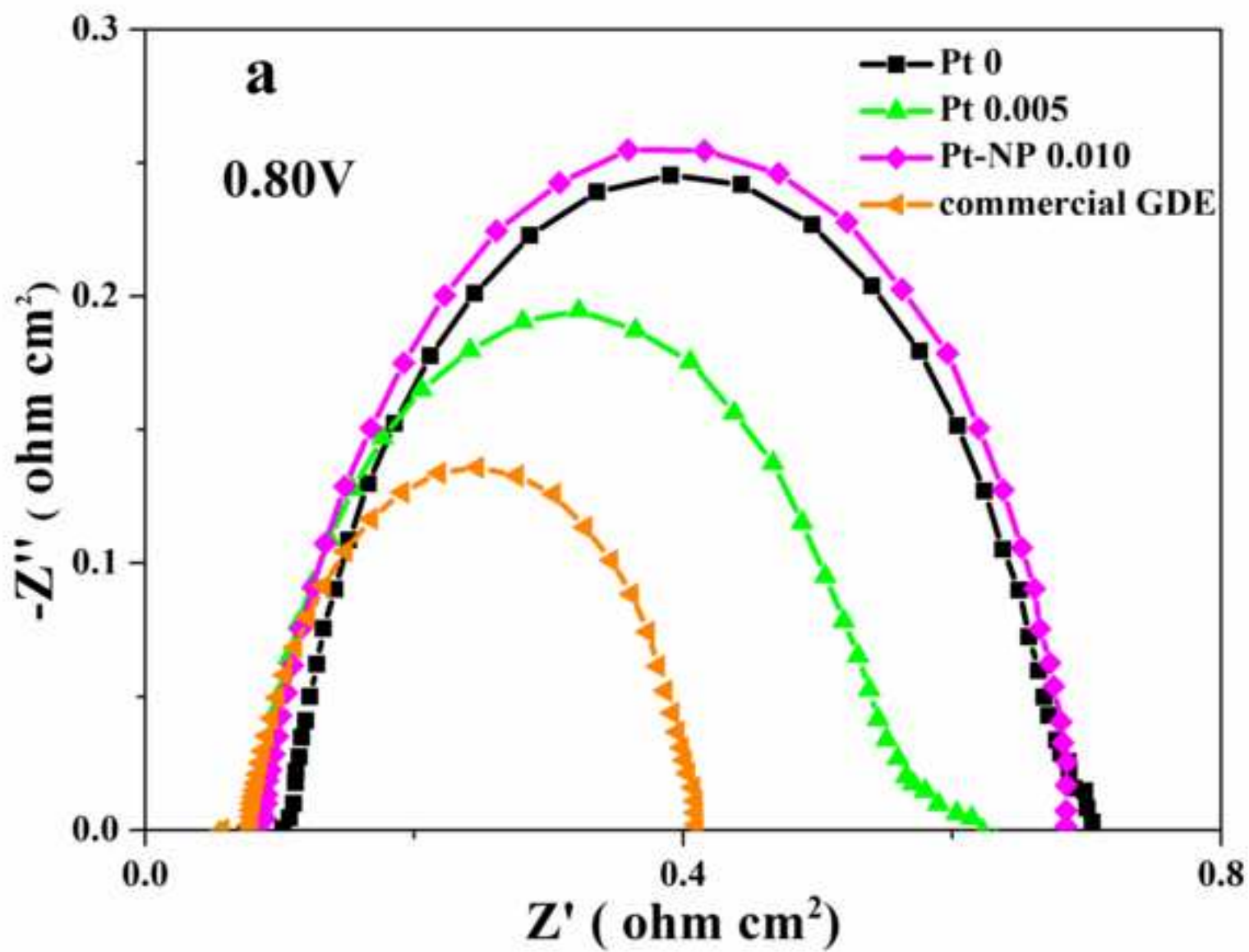


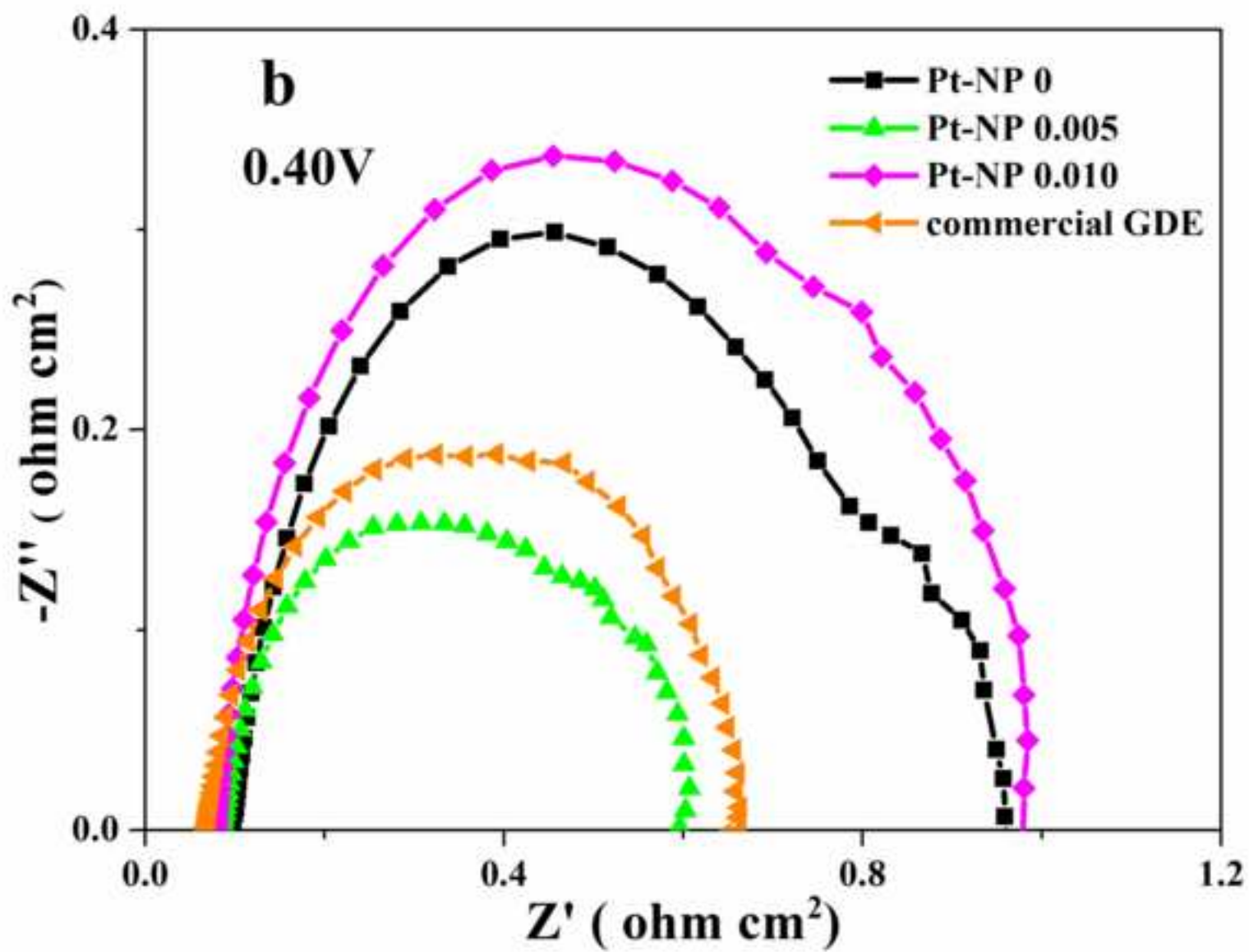
Figure 2  
[Click here to download high resolution image](#)













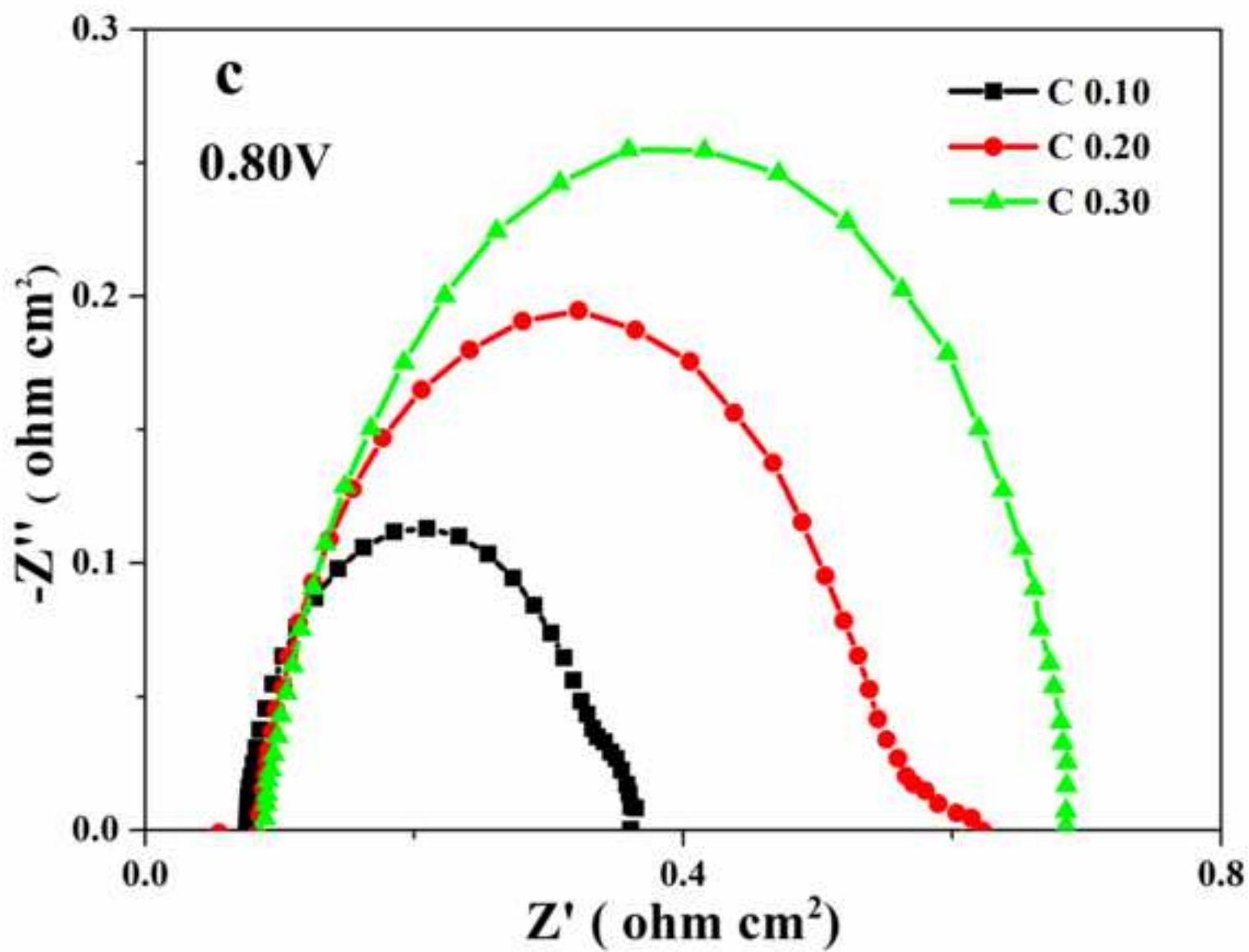
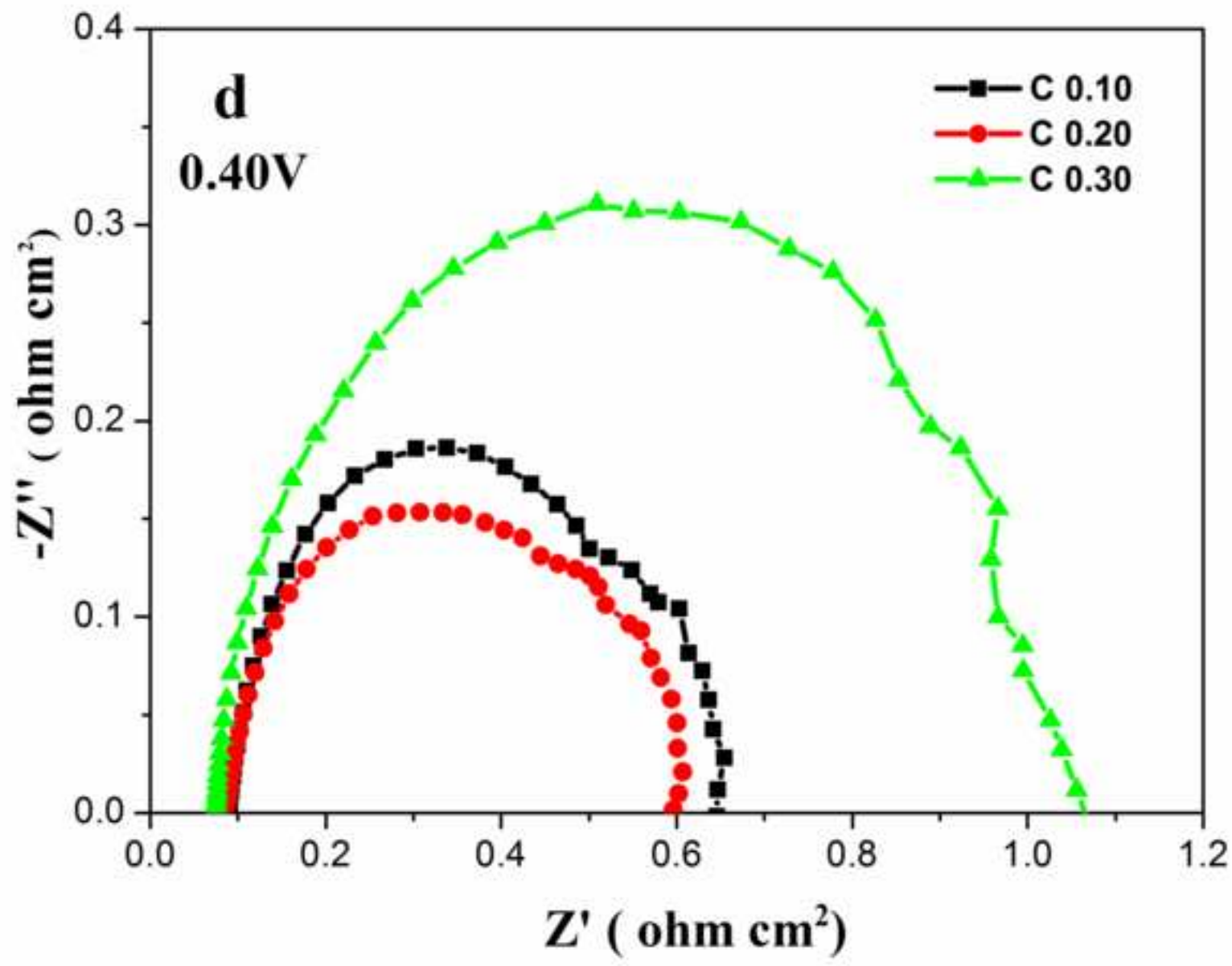
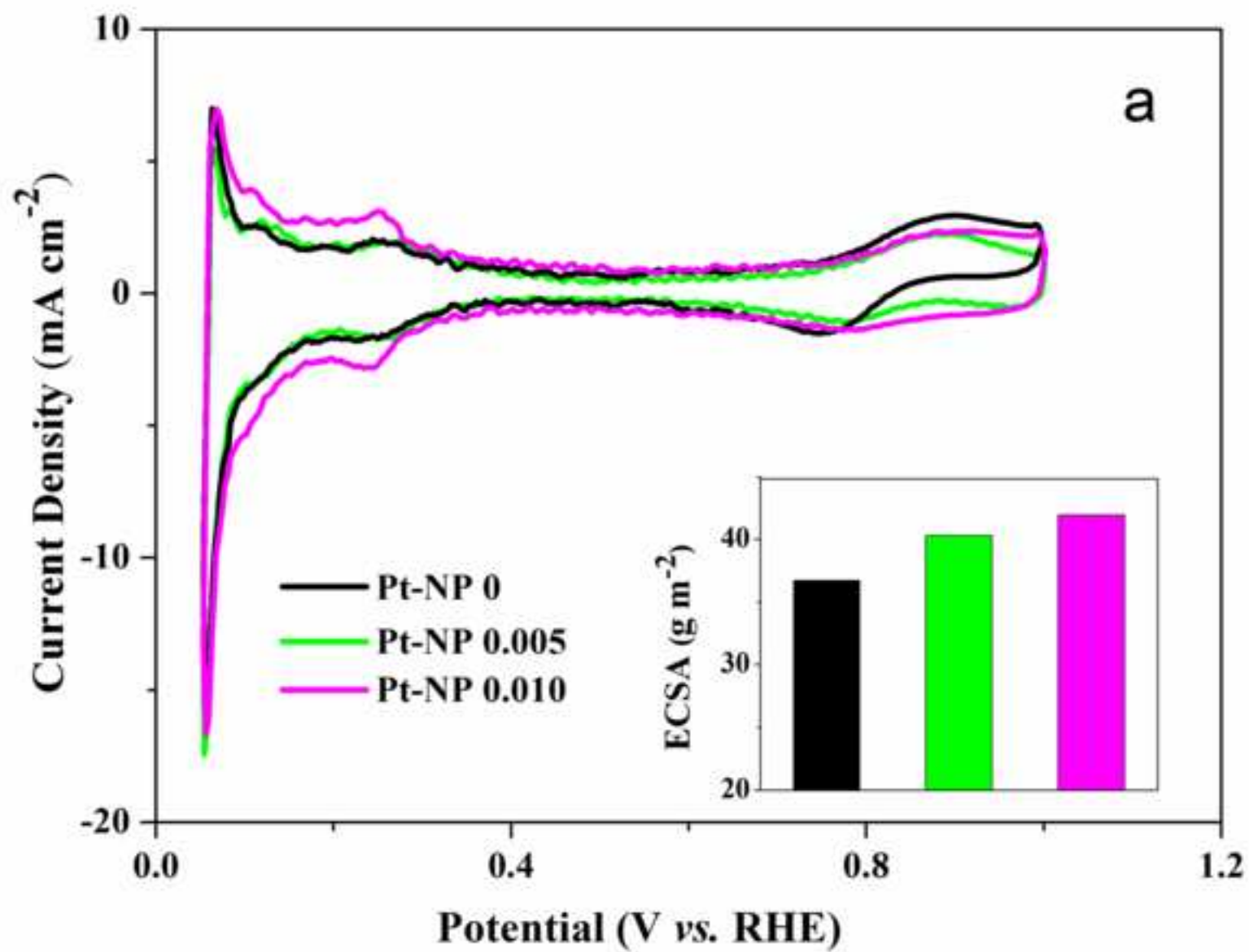


Figure 4(d)

[Click here to download high resolution image](#)





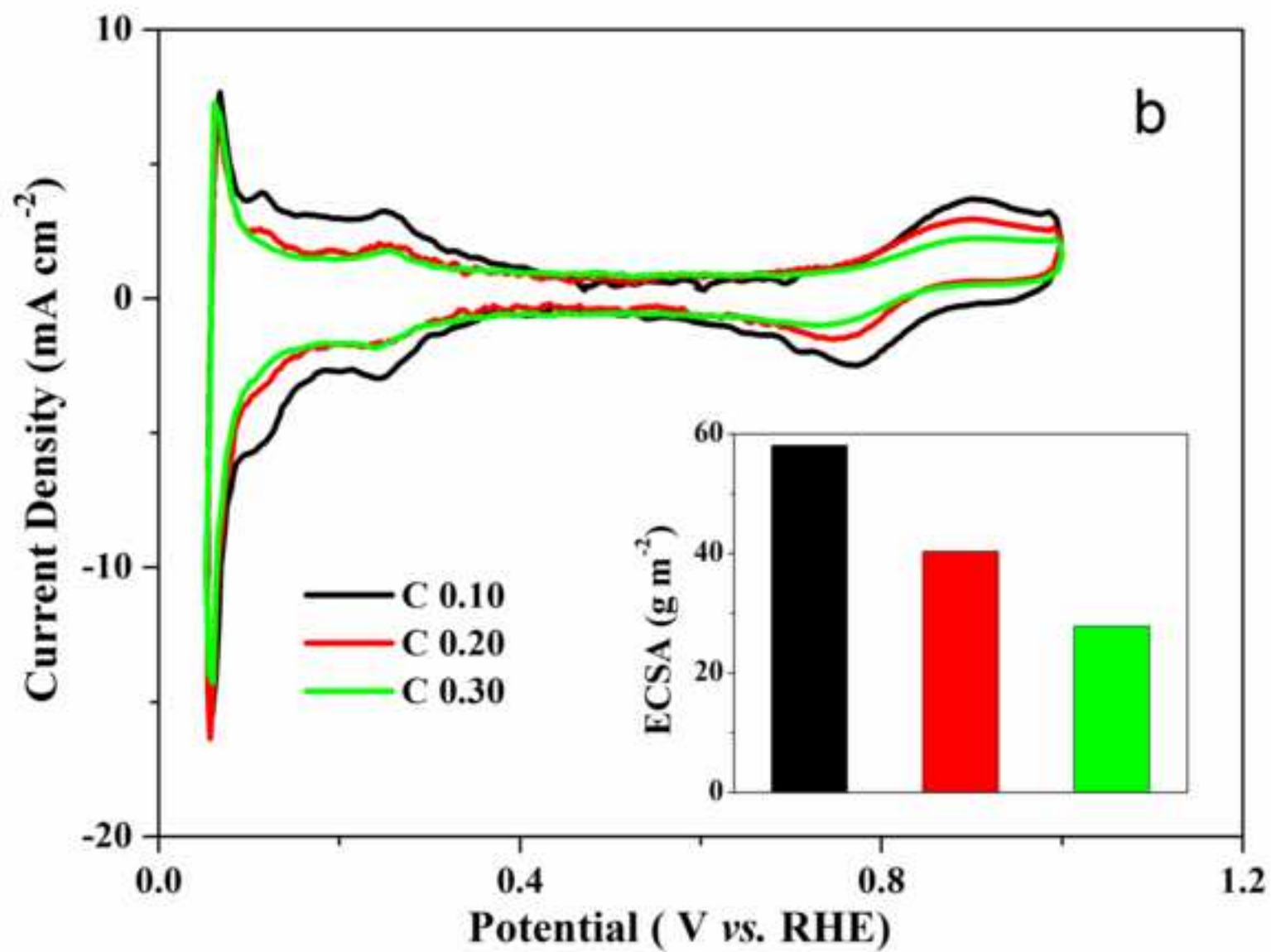
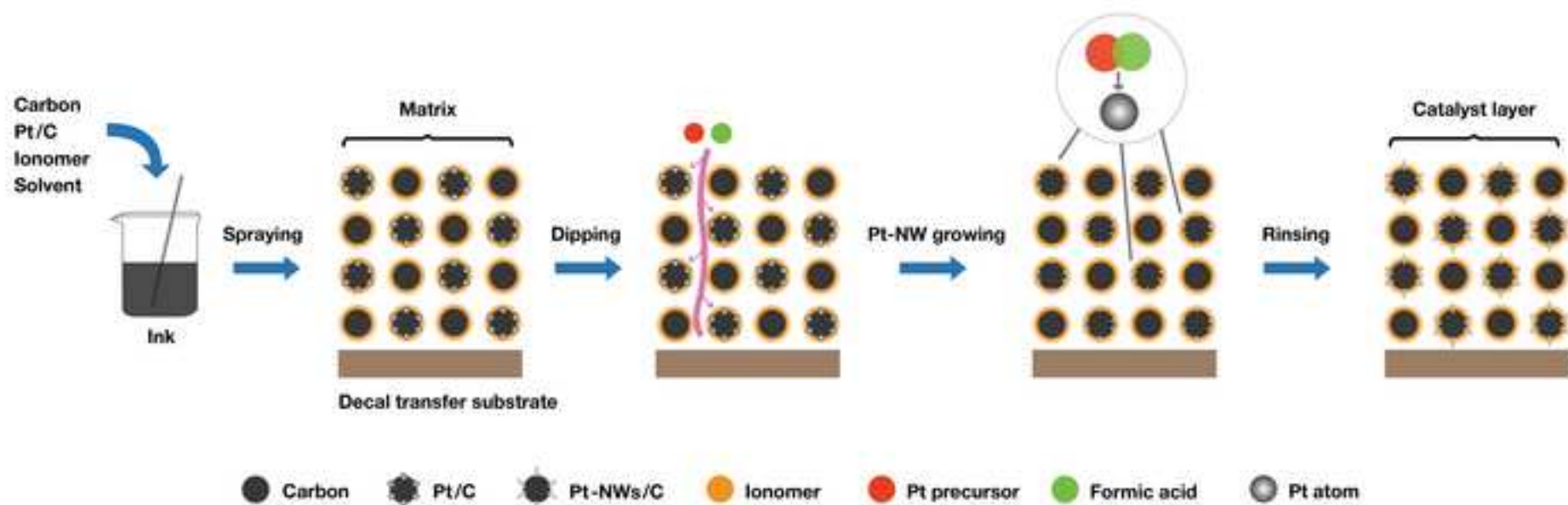


Figure 6  
[Click here to download high resolution image](#)



**Supplementary Material**

[Click here to download Supplementary Material: Figure Titles.docx](#)